NASA Technical Memorandum 4435

Hypersonic Lateral and Directional Stability Characteristics of Aeroassist Flight Experiment Configuration in Air and CF_4

John R. Micol and William L. Wells

MAY 1993

NASA Technical Memorandum 4435

Hypersonic Lateral and Directional Stability Characteristics of Aeroassist Flight Experiment Configuration in Air and CF_4

John R. Micol and William L. Wells
Langley Research Center
Hampton, Virginia

Summary

The proposed Aeroassist Flight Experiment (AFE) utilized a 14-ft-diameter raked and blunted elliptical cone to demonstrate the flight characteristics of space transfer vehicles (STV's). The AFE was to be carried to orbit by and launched from the Space Shuttle orbiter, where instrumentation for 10 on-board experiments would have obtained aerodynamic and aerothermodynamic data for velocities near 32 000 ft/sec at altitudes above 245 000 ft. A preflight ground-based test program was initiated to assess the aerodynamic and aerothermodynamic characteristics of the baseline concept and to provide benchmark data for calibration of computational fluid dynamics codes to be used in flight predictions. The data reported herein are results from one phase of this ground-based study. Static lateral and directional stability characteristics were obtained for the AFE configuration at angles of attack from $-10°$ to $10°$. Tests were conducted in air at Mach numbers of 6 and 10 and in tetrafluoromethane (CF_4) at Mach 6 to examine the effects of Mach number, Reynolds number, and normal-shock density ratio.

Changes in Mach number from 6 to 10 in air or in Reynolds number by a factor of 4 at Mach 6 had a negligible effect on the lateral and directional stability characteristics of the baseline AFE configuration. Variations in density ratio across the normal portion of the bow shock from approximately 5 (air) to 12 (CF_4) had a measurable effect on lateral and directional aerodynamic coefficients, but no significant effect on lateral and directional stability characteristics. The tests in air and CF_4 indicated that the configuration was laterally and directionally stable through the test range of angle of attack.

Unfortunately, the AFE program was cancelled in late 1991. The realization of an AFE flight in the future is possible but uncertain. Thus, this paper documents the lateral and directional aerodynamic characteristics of the baseline AFE vehicle for use in the design of future aeroassist space transfer vehicles.

Introduction

Among the space transportation systems proposed for the future are space transfer vehicles (STV's), which are designed to ferry cargo between higher Earth orbits (for example, geosynchronous and lunar orbits) and lower Earth orbit where the Space Shuttle and Space Station *Freedom* will operate. (This class of vehicle was formerly referred to as orbital transfer vehicles or OTV's.) Upon return of the vehicle from high Earth orbit, its velocity must be greatly reduced to attain a nearly circular low Earth orbit. This decrease in velocity can be achieved either by using retrorockets or by guiding the vehicle through a portion of the atmosphere and allowing aerodynamic drag forces to slow the vehicle. Studies have shown that lower propellant loads would be required for the aeroassist method (ref. 1); thus, payloads could be increased.

Future STV's that will be designed to use Earth atmosphere for deceleration are generally referred to as aeroassisted space transfer vehicles or ASTV's (formerly AOTV's). These vehicles will have high drag and a relatively low lift-to-drag ratio and will fly at very high altitudes and velocities throughout the atmospheric portion of the trajectory. Before the actual flight vehicle can be designed with optimal aerodynamic and aerothermodynamic characteristics, additional information about very high-altitude, high-velocity flight is required. To obtain such information, a subscale flight was proposed whereby a 14-ft-diameter ASTV configuration with 10 on-board experiments would be launched from the Space Shuttle and accelerated back into the atmosphere with a rocket. This Aeroassist Flight Experiment (AFE) would make a sweep through the atmosphere to an altitude of about 245 000 ft with a velocity of nearly 32 000 ft/sec to gain aerodynamic and aerothermal information and return to low Earth orbit for retrieval by the Space Shuttle. The on-board instrumentation would measure and record the aerodynamic characteristics and aerothermodynamic environment of this entry trajectory, and the data would be used to validate computational fluid dynamics (CFD) computer codes and ground-to-flight extrapolation of experimental data for use in future ASTV designs. This flight experiment was proposed because the high-velocity, low-density flow environment cannot be duplicated or simulated in present test facilities, nor can it be predicted with certainty by existing techniques.

Naturally, the AFE would require an extensive aerodynamic and aerothermodynamic experimental and computational data base for its design and successful flight. Present test facilities, in conjunction with the best CFD codes, would provide this information. For this reason, a preflight test program in ground-based hypersonic facilities (ref. 2) was initiated to develop the required aerodynamic and aerothermodynamic data base. This data base will be used to perform the first phase of CFD computer code calibration. The experimental results presented herein are part of an extensive ground-based test program performed at the Langley Research Center. Previous results are presented in references 3–6. The details of the rationale for the flight experiment are

outlined in reference 7, and the set of experiments to be performed is described in reference 8.

A primary concern for the AFE vehicle is the aerothermal heating on the fore- and aftbody thermal protection system (TPS). Because of these aerothermal concerns, low values of sideslip angles are desirable to minimize heating to the aftbody or payload and to prevent large thermal fluctuations on the heat shield. Thus, an accurate knowledge of the lateral and directional stability characteristics of the AFE is required. (Lateral and directional stability requirements for a low lift-to-drag aeromaneuvering vehicle are discussed in ref. 9.)

CFD codes are not generally used to provide aerodynamic information for vehicles at sideslip angles. Computed lateral and directional stability characteristics for the AFE would require calculations of the entire body at various sideslip angles, thus increasing computational time, complexity, and cost. Hence, determination of these stability characteristics for the flight vehicle must rely on experimental data obtained in ground-based facilities.

This paper addresses the effects of Mach number, Reynolds number, and normal-shock density ratio (a "real gas" simulation parameter) on lateral and directional aerodynamic characteristics measured on the baseline AFE configuration. Tests were conducted at Mach 6 and 10 in air and at Mach 6 in tetrafluoromethane (CF_4) through a range of angle of attack and sideslip.

During the continuum-flow portion of the flight, the AFE vehicle is expected to undergo normal-shock density ratios of about 18, whereas conventional hypersonic wind tunnels that use air or nitrogen as the test gas only produce ratios of 5 to 7. In flight, this large density ratio results from dissociation of air as it passes into the high-temperature shock layer. This real-gas effect may have a significant impact on shock detachment distance, distributions of heating and pressure, and aerodynamic characteristics (ref. 10).

For blunt bodies at hypersonic speeds, the primary factor that governs the shock stand-off distance and inviscid forebody flow is the normal-shock density ratio. (See ref. 10.) Certain aspects of a real gas can be simulated by the selection of a test gas that has a low ratio of specific heats and provides large values of density ratio. These conditions can be obtained in the Langley Hypersonic CF_4 Tunnel, which provides a simulation of this phenomenon by producing a density ratio of about 12 across the shock. This tunnel, in conjunction with the Langley 20-Inch Mach 6 Tunnel, provides the capability to test a given model at the same free-stream Mach number and Reynolds number, but at two values of density ratio (5.25 in air and 12.0 in CF_4). Thus, data for code calibration are provided that include the effects of normal-shock density ratio. Tests were performed in air at Mach 10 and through a range of Reynolds numbers at Mach 6 to verify that aerodynamic characteristics were independent of significant changes in Mach numbers and Reynolds numbers for the blunt AFE configuration in hypersonic continuum flow.

However, the AFE program cancellation ended the research efforts on this configuration. Thus, this paper documents the lateral and directional characteristics of the baseline AFE vehicle for use in the design of future aeroassist space transfer vehicles.

Symbols

C_l	rolling-moment coefficient, $\frac{\text{Rolling moment}}{q_\infty dS}$
C_{l_β}	$= \Delta C_l/\Delta\beta$, per deg
C_n	yawing-moment coefficient, $\frac{\text{Yawing moment}}{q_\infty dS}$
C_{n_β}	$= \Delta C_n/\Delta\beta$, per deg
C_y	side-force coefficient, $\frac{\text{Side force}}{q_\infty S}$
C_{y_β}	$= \Delta C_y/\Delta\beta$, per deg
d	model length in symmetry plane, in.
M	Mach number
p	pressure, psia
q	dynamic pressure, psia
Re_∞	unit free-stream Reynolds number, ft^{-1}
$Re_{2,d}$	postshock Reynolds number based on d
S	reference area, model base area, in^2 (10.604 in^2 when $d = 3.67$ in. and 4.936 in^2 when $d = 2.50$ in.)
T	temperature, °R
U	velocity, ft/sec
$\overline{X}$	moment transfer distance in axial direction (fig. 4), in. (1.673 in. when $d = 3.67$ in. and 1.559 in. when $d = 2.50$ in.)
x, y, z	axial, lateral, and vertical coordinates for AFE (fig. 4)

$\overline{Z}$	moment transfer distance in normal direction (fig. 4), in. (0.129 in. when $d = 3.67$ in. and 0.0979 in. when $d = 2.50$ in.)
α	angle of attack, deg
β	angle of sideslip, deg
γ	ratio of specific heats of the test gas
ρ	density of the test gas, lbm/in^3

Subscripts:

t	total conditions
∞	free-stream conditions
2	conditions behind the normal shock

AFE Configuration

The AFE flight vehicle would consist of a 14-ft-diameter drag brake, an instrument carrier at the base, a solid-rocket propulsion motor, and small control motors. A sketch of the vehicle is shown in figure 1. The drag brake (fig. 2), which is the forebody configuration, is derived from a blunted 60° half-angle elliptical cone that is raked at 73° to the cone centerline to produce a circular raked plane. A skirt with an arc radius equal to one-tenth the rake-plane diameter and with an arc length corresponding to 60° has been attached to the rake plane to reduce aerodynamic heating around the base periphery. The blunt nose is an ellipsoid with an ellipticity equal to 2.0 in the symmetry plane. The ellipsoid nose and the skirt are at a tangent at their respective intersections to the elliptical cone surface. A detailed description of the forebody analytical shape is presented in reference 11.

Apparatus and Tests

Facilities

Langley 31-Inch Mach 10 Tunnel. The Langley 31-Inch Mach 10 Tunnel (formerly the Langley Continuous Flow Hypersonic Tunnel) expands dry air through a three-dimensional contoured nozzle to a 31-in-square test section to achieve a nominal Mach number of 10. The air is heated to approximately 1850°R by an electrical resistance heater, and the maximum reservoir pressure is approximately 1500 psia. The tunnel operates in the blowdown mode with run times of approximately 60 sec. Force and moment data can be obtained through a range of angle of attack or sideslip during one run by utilization of the pitch-pause capability of the model support system. This tunnel is described in more detail in reference 12.

Langley 20-Inch Mach 6 Tunnel. The 20-Inch Mach 6 Tunnel is a blowdown wind tunnel that uses dry air as the test gas. The air may be heated to a maximum temperature of approximately 1100°R by an electrical resistance heater; the maximum reservoir pressure is 525 psia. A fixed-geometry, two-dimensional, contoured nozzle with parallel side walls expands the flow to a Mach number of 6 at the 20-in-square test section. The model injection mechanism allows changes in angle of attack and sideslip during a run. Run durations are usually 60 to 120 sec, although longer times can be attained by connection to auxiliary vacuum storage. A description of this facility and the calibration results are presented in reference 13.

Langley 20-Inch Mach 6 CF_4 Tunnel. The 20-Inch Mach 6 CF_4 Tunnel is a blowdown wind tunnel that uses CF_4 as the test gas. The CF_4 can be heated to a maximum temperature of 1530°R by two molten lead bath heat exchangers connected in parallel. The maximum pressure in the tunnel reservoir is 2600 psia. Flow is expanded through an axisymmetric, contoured nozzle designed to generate a Mach number of 6 at the 20-in-diameter exit. This facility has an open-jet test section. Run duration can be as long as 30 sec, but 10 sec is sufficient for most tests because the model injection system is not presently capable of changing angle of attack or sideslip during a run. A detailed description of the 20-Inch Mach 6 CF_4 tunnel is presented in reference 14.

Just before the present test series, the tunnel was modified extensively. Included in those modifications were a new nozzle, a new test section and model injection system, a new diffuser, and improvements in wiring of the controls and of the data acquisition system. The new nozzle was designed to improve flow quality along the centerline and to more closely match the Mach number in the Mach 6 air tunnel that is often used to produce data for comparison with the CF_4 data. Calibration results (ref. 15) that were obtained after the new nozzle was installed indicate greatly improved flow uniformity near the nozzle centerline. For the present test series, the model was tested on the tunnel centerline. Previously, models were tested off centerline to avoid flow disturbances. (See ref. 14.)

Models

Two aerodynamic models were fabricated and tested. The models were identical except for size; the base heights (d in fig. 2) at the symmetry plane were 3.67 in. (2.2 percent scale) as shown in figure 3(a) and 2.50 in. (1.5 percent scale) as shown in figure 3(b). The 3.67-in-diameter model is made in three parts—a stainless steel forebody (aerobrake), an aluminum aftbody (instrument carrier and propulsion motor), and a stainless steel balance holder. The 2.50-in-diameter model, shown mounted in the Langley 20-Inch Mach 6 CF_4 Tunnel in figure 3(c), is fabricated of aluminum and does not include the circular or hexagonally shaped aftbody and the simulated propulsion motor of previous models that were tested (ref. 16). A cylinder protrudes from the base to accept the balance. The acute angle between the balance and cylinder axis and the base in the symmetry plane is 73°. The 2.50-in-diameter model was fabricated to provide an air gap between the end of the balance and the end of the cavity in the forebody; its purpose was to reduce conductive heating. For both models, shrouds were built to shield the balance from base-flow closure. The shrouds attach to the sting, and clearance was provided to avoid interference with the balance during model movement when forces and moments were applied. The forebodies were machined to the design size and shape within a tolerance of ± 0.003 in. Angle of attack (see fig. 2) and sideslip (see fig. 4) in this paper are referenced to the axis of the original elliptical cone.

Instrumentation

Aerodynamic force and moment data were measured with sting-supported, six-component, water-cooled, internal strain gauge balances. Two thermocouples were installed in the water jacket that surrounds the measuring elements to monitor internal balance temperatures. The load rating for each component of the two balances (one for each model size) is presented in table I. The calibration accuracy is 0.5 percent of the maximum load rating for each component.

Test Conditions

The tests were conducted at nominal free-stream Mach numbers of 6 and 10 in air and at Mach 6 in CF_4. (Nominal test conditions are presented in table II.) The angles of attack for Mach 6 in air were 0° and ±5° with nominal sideslip angles of 0°, −2°, and −4°. Tests at Mach 6 in CF_4 were at angles of attack of 0°, ±5°, and ±10° with nominal sideslip angles of 0°, ±2.5°, and ±5°; at Mach 10 (except for $\alpha = -2.5°$, where only a negative β sweep was performed), the angles of attack were 0°, ±2.5°, ±5°, and ±10° with nominal sideslip angles of 0°, ±2°, and ±4°.

Test Procedures

Blunt models are conducive to heat conduction through the forebody face during a run, which generally produces a gradual increase in temperature gradients along the balance even though the balance is water cooled. Because temperature gradients were not accounted for in the laboratory calibration of the balance, efforts were made to minimize these gradients by limiting the test times. In the 20-Inch Mach 6 CF_4 Tunnel, the model was mounted at the desired angle of attack and sideslip before the run. After the test-stream flow was established, the model was injected to the test-stream centerline. Data were gathered for approximately 5 sec, then the model was retracted. In the air tunnels, the model was mounted at $\alpha = \beta = 0°$ before the run. After test-stream flow was established, the model was injected to the stream centerline, then pitched to the next angle of attack (or sideslip angle) by the pitch-pause mechanism. Data were taken while the model was stationary at each position. The balance thermocouples were monitored during each run to assure that the temperature gradient within the balance remained within an acceptable limit. Typical run times for a set of α and β sweeps in the air facilities were about 15 sec.

Data Reduction and Uncertainty

Each of the three test facilities has a dedicated stand-alone data system. Output signals from the balances were sampled and digitized by an analog-to-digital converter, then stored and processed by a computer. The analog signals were sampled at a rate of 50 per second in the Mach 6 CF_4 and Mach 10 air tunnels and at 20 per second in the Mach 6 air tunnel. A single value of data reported herein represents an average of values measured for 2 sec in the Mach 6 CF_4 and Mach 6 air tunnels and for 0.5 sec in the Mach 10 air tunnel. Corrections were made for model tare weights at each angle of attack and for interactions between different elements of the balances. Corrections were not made for base pressures.

Balance-related calculated uncertainties in the measured static aerodynamic coefficients are given in table III. These uncertainties are based on balance output signals related to forces and moments by a laboratory calibration that is accurate to ±0.5 percent of the rated load for each component. (See table I.) For the AFE, the moment reference center is

located at the center of the rake plane. (See fig. 4.) Thus, moments reduced about the model rake-plane center and reported herein have greater uncertainties than those measured at the balance moment center. The yawing and rolling moments at the balance have an uncertainty of only ±0.5 percent of the rated load, whereas the moment at the rake-plane center also includes uncertainties associated with the forces in the transfer equation. The transfer equation is

$$\text{Yawing moment}_{RP} = \text{Yawing moment}_{B} - (\overline{X})\ \text{(Side force)}$$

and

$$\text{Rolling moment}_{RP} = \text{Rolling moment}_{B} - (\overline{Z})\ \text{(Side force)}$$

where the subscripts RP and B denote the rake-plane center and the balance moment center, respectively. The transfer distances $\overline{X}$ and $\overline{Z}$ are defined in figure 4. In coefficient form, the uncertainty Δ related to the balance calibration for the side force is

$$\Delta C_y = \frac{\pm(0.005)\ \text{(Force rating)}}{q_\infty S}$$

The uncertainty for the yawing moment is

$$\Delta C_{n,B} = \frac{\pm(0.005)\ \text{(Moment rating)}}{q_\infty d S}$$

and an identical equation applies for the rolling moment. These balance uncertainties are sufficient for measurements at the balance moment center. However, at the rake-plane center, the yawing-moment uncertainty is

$$\Delta C_{n,RP} = \pm\left[(\Delta C_{n,B})^2 + \left(\Delta C_y \frac{\overline{X}}{d}\right)^2\right]^{0.5}$$

and the rolling-moment uncertainty is

$$\Delta C_{l,RP} = \pm\left[(\Delta C_{l,B})^2 + \left(\Delta C_y \frac{\overline{Z}}{d}\right)^2\right]^{0.5}$$

Note that all the terms include the free-stream dynamic pressure in the denominator so that the uncertainties are less at test conditions where q_∞ is large—that is, at a higher Reynolds number rather than at a lower Reynolds number. The uncertainty in dynamic pressure is ±3 percent. The flow conditions for which the present uncertainties have been calculated are presented in table II.

Results and Discussions

The aerodynamic data from the Mach 10 air tests are tabulated in table IV. The Mach 6 results are presented in tables V and VI for air and in table VII for CF_4. The test Reynolds number and model diameter are indicated in each table title.

The aerodynamic coefficients C_y, C_n, and C_l are plotted for an angle-of-sideslip range at various angles of attack in each facility and presented in figures 5–7 for Mach 10 in air, Mach 6 in air, and Mach 6 in CF_4, respectively. Data obtained at Mach 6 in air (fig. 6) indicated no effect of Reynolds number on measured lateral and directional coefficients for a factor-of-4 increase in postshock Reynolds number. (Similar trends with respect to Reynolds number were also observed for AFE longitudinal aerodynamic characteristics presented in ref. 16 in which a negligible effect of Reynolds number was noted for Mach 6 and 10 in air and at Mach 6 in CF_4.) Therefore, the assumption is made that the effect of Reynolds number on measured lateral and directional data at Mach 10 in air and Mach 6 in CF_4 is also negligible. The data are amenable to linear curve fits as shown in figures 5–7, for which the ordinate scale is quite sensitive. These curves would be expected to go through the origin because the model was symmetrical about the pitch plane. However, as observed in figures 5–7, an offset exists. This offset may be attributed to model misalignment or to any small stray signal in the data system that could cause a constant data offset because of the very small values being measured relative to the load range of the balance.

For example, if a slight misalignment of the model in the roll direction were introduced during model setup or if the balance location within the model were slightly misaligned, thereby producing a small offset in the center of gravity location (that is, within a few thousandths of an inch) in the side plane (y direction in fig. 4), then the effect of the large axial-force component on this small moment arm may produce a continuous bias in the measured quantities. For instance, from reference 16 at $\alpha = \beta = 0°$, $Re_\infty = 0.46 \times 10^6$/ft, and Mach 6 in CF_4, the axial-force coefficient is 1.382. The yawing-moment coefficient, from table VII for similar conditions, is 0.004. In much the same way as the change in the center of pressure in longitudinal aerodynamics is located, forming the ratio of yawing-moment coefficient to axial-force coefficient yields the moment arm in the y direction, which for this case is approximately 0.003 in. and thus within acceptable fabrication tolerances. A second linear curve, parallel to the data-faired curve, is drawn through the origin in

each part of figures 5–7. Values from measurements and the curve through the origin of figures 5–7 are presented in tables IV–VII. Use of the slopes of these parallel curves through the origin to represent the lateral and directional stability derivatives should be valid because the data curves are linear through the test sideslip range.

The lateral and directional stability derivatives are presented in figure 8 and table VIII through the range of angle of attack for which tests were performed in each facility. For all test conditions, the configuration was laterally and directionally stable, as indicated by the positive values of C_{n_β} and negative values of C_{l_β}. A comparison of lateral and directional stability derivatives obtained at Mach numbers of 6 and 10 in air illustrates no significant effect of Mach number on stability characteristics; a comparison of these stability derivatives with those obtained at Mach 6 in CF_4 indicates a small but measurable effect of normal-shock density ratio on lateral and directional stability characteristics. Although the numerical values for air and CF_4 are not greatly different, the data trends in air and CF_4 appear to be opposite. (Similar trends were observed in the longitudinal aerodynamic characteristics discussed in ref. 16.) This trend is most obvious for C_{l_β}, wherein the small numerical values require an expanded scale on the graph. The wind tunnel results in CF_4 are believed to be a better simulation of flight data than those in air because the shock detachment distance for CF_4 is closer to the distance predicted for the actual flight case. (For example, see refs. 6 and 16.)

Concluding Remarks

Static lateral and directional stability characteristics were obtained for the Aeroassist Flight Experiment (AFE) configuration through a range of angle of attack from $-10°$ to $10°$. Tests were conducted on two different-sized models at Mach numbers of 6 and 10 in air and at a Mach number of 6 in tetrafluoromethane (CF_4). The effects of Mach number, Reynolds number, and normal-shock density ratio on lateral and directional stability characteristics were examined.

Changes in Mach number from 6 to 10 in air or in Reynolds number by a factor of 4 at Mach 6 had a negligible effect on the lateral and directional stability characteristics of the baseline AFE configuration. Variations in density ratio across the normal portion of the bow shock from approximately 5 (air) to 12 (CF_4) had a measurable effect on lateral and directional aerodynamic coefficients, but no significant effect on lateral and directional stability characteristics. The tests in air and CF_4 indicated that the configuration is laterally and directionally stable through the test range of angle of attack as indicated by the positive values of C_{n_β} and negative values of C_{l_β} (positive effective dihedral).

In late 1991, the AFE program was cancelled and thus ended research efforts on this configuration. The realization of an AFE flight in the future is possible but uncertain. Hence, this paper documents the lateral and directional aerodynamic characteristics of the baseline AFE vehicle for use in the design of future aeroassist space transfer vehicles.

NASA Langley Research Center
Hampton, VA 23681-0001
March 25, 1993

References

1. Walberg, Gerald D.: A Review of Aeroassisted Orbit Transfer. AIAA-82-1378, Aug. 1982.

2. Wells, William L.: Wind-Tunnel Preflight Test Program for Aeroassist Flight Experiment. *Technical Papers—AIAA Atmospheric Flight Mechanics Conference,* Aug. 1987, pp. 151–163. (Available as AIAA-87-2367.)

3. Wells, William L.: *Free-Shear-Layer Turning Angle in Wake of Aeroassist Flight Experiment (AFE) Vehicle at Incidence in M = 10 Air and M = 6 CF_4.* NASA TM-100479, 1988.

4. Micol, John R.: Experimental and Predicted Pressure and Heating Distributions for Aeroassist Flight Experiment Vehicle. *J. Thermophys. & Heat Transf.,* July–Sept. 1991, pp. 301–307.

5. Wells, William L.: *Surface Flow and Heating Distributions on a Cylinder in Near Wake of Aeroassist Flight Experiment (AFE) Configuration at Incidence in Mach 10 Air.* NASA TP-2954, 1990.

6. Micol, John R.: *Simulation of Real-Gas Effects on Pressure Distributions for Aeroassist Flight Experiment Vehicle and Comparison With Prediction.* NASA TP-3157, 1992.

7. Jones, Jim J.: The Rationale for an Aeroassist Flight Experiment. AIAA-87-1508, June 1987.

8. Walberg, G. D.; Siemers, P. M., III; Calloway, R. L.; and Jones, J. J.: The Aeroassist Flight Experiment. IAF Paper 87-197, Oct. 1987.

9. Gamble, Joe D.; Spratlin, Kenneth M.; and Skalecki, Lisa M.: Lateral Directional Requirements for a Low L/D Aeromaneuvering Orbital Transfer Vehicle. *A Collection of Technical Papers—AIAA Atmospheric Flight Mechanics Conference,* Aug. 1984, pp. 402–413. (Available as AIAA-84-2123.)

10. Jones, Robert A.; and Hunt, James L. (appendix A by James L. Hunt, Kathryn A. Smith, and Robert B. Reynolds and appendix B by James L. Hunt and Lillian R. Boney): *Use of Tetrafluoromethane To Simulate Real-Gas Effects on the Hypersonic Aerodynamics of Blunt Vehicles.* NASA TR R-312, 1969.

11. Cheatwood, F. McNeil; DeJarnette, Fred R.; and Hamilton, H. Harris, II: *Geometrical Description for a Proposed Aeroassisted Flight Experiment Vehicle.* NASA TM-87714, 1986.

12. Miller, C. G.: Langley Hypersonic Aerodynamic/ Aerothermodynamic Testing Capabilities—Present and Future. AIAA-90-1376, June 1990.

13. Miller, Charles G., III; and Gnoffo, Peter A.: *Pressure Distributions and Shock Shapes for 12.84°/7° On-Axis and Bent-Nose Biconics in Air at Mach 6.* NASA TM-83222, 1981.

14. Midden, Raymond E.; and Miller, Charles G., III: *Description and Calibration of the Langley Hypersonic CF_4 Tunnel—A Facility for Simulating Low γ Flow as Occurs for a Real Gas.* NASA TP-2384, 1985.

15. Micol, John R.; Midden, Raymond E.; and Miller, Charles G., III: Langley 20-Inch Hypersonic CF_4 Tunnel: A Facility for Simulating Real-Gas Effects. AIAA-92-3939, July 1992.

16. Wells, William L.: *Measured and Predicted Aerodynamic Coefficients and Shock Shapes for Aeroassist Flight Experiment (AFE) Configuration.* NASA TP-2956, 1990.

Table I. Balance Load Ratings Used in Tests

Model size, in.	Load rating		
	Side, lbf	Roll, in-lbf	Yaw, in-lbf
2.50	3	2	3
3.67	15	10	15

Table II. Nominal Test Conditions

Re_∞, ft^{-1}	p_t, lbf/in^2	T_t, °R	p_∞, lbf/in^2	T_∞, °R	M_∞	U_∞, ft/sec	q_∞, lbf/in^2	ρ_2/ρ_∞	Re_2, ft^{-1}	$p_{t,2}$, lbf/in^2	$T_{t,2}$, °R	γ_2
Langley 31-Inch Mach 10 Tunnel; air as test gas												
1.09×10^6	700	1810	0.0175	91.7	9.90	4651	1.20	6.0	0.87×10^5	2.23	1810	1.34
Langley 20-Inch Mach 6 Tunnel; air as test gas												
0.63×10^6	30	845	0.023	108.3	5.84	2975	0.54	5.2	0.96×10^5	1.00	845	1.40
2.21	126	910	.084	112.5	5.94	3095	2.10	5.2	3.50	3.86	910	1.40
Langley 20-Inch Mach 6 Tunnel; CF_4 as test gas												
0.46×10^6	1515	1280	0.063	386	5.87	3000	1.29	11.8	1.77	2.54	1271	1.10

Table III. Balance-Related Uncertainties in Experimental Lateral and Directional Aerodynamic Coefficients

$Re_{2,d}$	d, in.	ΔC_l, ±	ΔC_n, ±	ΔC_y, ±
$M_\infty = 10$; air as test gas				
18 042	2.50	0.0007	0.0019	0.0025
$M_\infty = 6$; air as test gas				
29 400	3.67	0.0024	0.0069	0.0131
107 000	3.67	.0006	.0018	.0034
$M_\infty = 6$; CF_4 as test gas				
37 000	2.50	0.0006	0.0017	0.0023

Table IV. Measured Lateral and Directional Aerodynamic Characteristics in Air for $M_\infty = 9.90, Re_\infty = 1.09 \times 10^6/\text{ft}, Re_{2,d} = 18\,042,$ and $d = 2.50$ in.

[Numbers with asterisk are derived from curve through 0,0 in fig. 5]

(a) $\alpha = 0°$

β, deg	C_l	C_n	C_y
−0.019	0.00096	0.00161	0.00826
.098	.00101	.00328	.00273
−.024	.00126	.00197	.00562
−.019	.00111	.00181	.00775
−.015	.00138	.00259	.00314
−.054	.00103	.00252	.00650
−.031	.00155	.00306	.00327
.052	.00171	.00375	.00386
−2.113	.00281	−.00248	.01521
−2.157	.00309	−.00152	.01305
−2.063	.00251	−.00169	.01238
−2.085	.00308	−.00103	.01323
2.242	−.00041	.00589	−.00079
2.099	−.00021	.00597	.00098
2.225	−.00034	.00676	−.00464
2.075	−.00039	.00667	−.00221
−4.296	.00426	−.00666	.02418
−4.302	.00463	−.00520	.02051
4.364	−.00173	.01030	−.00987
4.350	−.00171	.01058	−.01067
0*	0*	0*	0*
−2.0*	.00145*	−.00377*	.00740*
2.0*	−.00145*	.00377*	−.00740*
−4.0*	.00290*	−.00755*	.01480*
4.0*	−.00290*	.00755*	−.01480*

Table IV. Continued

(b) $\alpha = 2.5°$

β, deg	C_l	C_n	C_y
−0.011	0.00104	0.00188	0.00692
−2.114	.00282	.00222	.01328
−4.316	.00438	.00699	.02341
−2.090	.00253	.00221	.01468
.065	.00101	.00241	.00591
−.017	.00110	.00192	.00554
2.233	−.00032	.00632	−.00226
4.410	−.00228	.01057	−.00934
2.130	−.00071	.00645	−.00284
−.003	.00126	.00282	.00379
0*	0*	0*	0*
−2.0*	.00152*	−.00402*	.00757*
2.0*	−.00152*	.00402*	−.00757*
−4.0*	.00304*	−.00804*	.01514*
4.0*	−.00304*	.00804*	−.01514*

(c) $\alpha = -2.5°$

β, deg	C_l	C_n	C_y
−0.022	0.00126	0.00219	0.00426
−2.169	.00240	−.00261	.01508
−4.280	.00425	−.00626	.02186
−2.083	.00262	−.00168	.01270
.055	.00111	.00265	.00359
0*	0*	0*	0*
−2.0*	.00140*	−.00408*	.00850*
−4.0*	.00280*	−.00816*	.01700*

Table IV. Continued

(d) $\alpha = 5.0°$

β, deg	C_l	C_n	C_y
−0.006	0.00116	0.00181	0.00645
2.245	−.00057	.00682	−.00293
4.380	−.00225	.01168	−.01189
2.076	−.00048	.00674	−.00302
−.037	.00113	.00227	.00667
−.013	.00136	.00206	.00528
−2.113	.00307	−.00308	.01548
−4.252	.00479	−.00775	.02400
−1.998	.00293	−.00254	.01485
.078	.00122	.00251	.00536
0*	0*	0*	0*
−2.0*	.00164*	−.00452*	.00841*
2.0*	−.00164*	.00452*	−.00841*
−4.0*	.00328*	−.00903*	.01681*
4.0*	−.00328*	.00903*	−.01681*

(e) $\alpha = -5.0°$

β, deg	C_l	C_n	C_y
−0.027	0.00127	0.00182	0.00544
2.191	−.00045	.00664	−.00389
4.379	−.00191	.01057	−.01165
2.050	−.00036	.00660	−.00391
−.065	.00120	.00249	.00389
−.018	.00128	.00202	.00500
−2.155	.00266	−.00198	.01200
−4.319	.00394	−.00607	.02079
−2.057	.00245	−.00172	.01178
.055	.00092	.00225	.00498
0*	0*	0*	0*
−2.0*	.00136*	−.00388*	.00746*
2.0*	−.00136*	.00388*	−.00746*
−4.0*	.00273*	−.00777*	.01492*
4.0*	−.00273*	.00777*	−.01492*

Table IV. Concluded

(f) $\alpha = 10.0°$

β, deg	C_l	C_n	C_y
−0.015	0.00071	0.00167	0.00508
2.237	−.00148	.00798	−.00585
4.334	−.00346	.01335	−.01427
2.096	−.00152	.00780	−.00523
.004	.00065	.00264	.00383
−.015	.00040	.00224	.00421
−2.068	.00260	−.00342	.01295
−4.203	.00417	−.00868	.02153
−2.012	.00227	−.00260	.01033
.114	.00011	.00331	.00200
0*	0*	0*	0*
−2.0*	.00182*	−.00517*	.00833*
2.0*	−.00182*	.00517*	−.00833*
−4.0*	.00363*	−.01034*	.01665*
4.0*	−.00363*	.01034*	−.01665*

(g) $\alpha = -10.0°$

β, deg	C_l	C_n	C_y
−0.017	0.00145	0.00066	0.00584
2.209	−.00054	.00590	−.00347
4.289	−.00228	.01080	−.01404
2.104	−.00053	.00669	−.00536
.011	.00119	.00212	.00217
−.015	.00123	.00056	.00612
−2.141	.00311	−.00414	.01723
−4.201	.00472	−.00836	.02457
−1.999	.00303	−.00340	.01536
.098	.00129	.00192	.00446
0*	0*	0*	0*
−2.0*	.00167*	−.00460*	.00933*
2.0*	−.00167*	.00460*	−.00933*
−4.0*	.00334*	−.00920*	.01865*
4.0*	−.00334*	.00920*	−.01865*

Table V. Measured Lateral and Directional Aerodynamic Characteristics in Air for $M_\infty = 5.84$, $Re_\infty = 0.63 \times 10^6$/ft, $Re_{2,d} = 29\,400$, and $d = 3.67$ in.

[Numbers with asterisk are derived from curve through 0,0 in fig. 6]

(a) $\alpha = 0°$

β, deg	C_l	C_n	C_y
0.0	−0.0004	0.0003	0.0018
−2.0	.0010	−.0036	.0093
−4.0	.0026	−.0078	.0176
0*	0*	0*	0*
−2.0*	.0015*	−.0043*	.0080*
−4.0*	.0030*	−.0085*	.0159*

(b) $\alpha = 5°$

β, deg	C_l	C_n	C_y
0.0	−0.0003	0.0006	0.0022
−2.0	.0013	−.0040	.0102
−4.0	.0031	−.0086	.0183
0*	0*	0*	0*
−2.0*	.0017*	−.0046*	.0079*
−4.0*	.0034*	−.0092*	.0158*

(c) $\alpha = -5°$

β, deg	C_l	C_n	C_y
0.0	−0.0004	0.0007	0.0018
−2.0	.0012	−.0036	.0101
−4.0	.0027	−.0078	.0184
0*	0*	0*	0*
−2.0*	.0015*	−.0041*	.0080*
−4.0*	.0030*	−.0081*	.0160*

Table VI. Measured Lateral and Directional Aerodynamic Characteristics in Air for $M_\infty = 5.94$, $Re_\infty = 2.21 \times 10^6$/ft, $Re_{2,d} = 107\,000$, and $d = 3.67$ in.

[Numbers with asterisk are derived from curve through 0,0 in fig. 6]

(a) $\alpha = 0°$

β, deg	C_l	C_n	C_y
0.0	−0.0002	0.0004	0.0018
−2.0	.0014	−.0039	.0097
−4.0	.0030	−.0082	.0178
0*	0*	0*	0*
−2.0*	.0015*	−.0043*	.0080*
−4.0*	.0030*	−.0085*	.0159*

(b) $\alpha = 5°$

β, deg	C_l	C_n	C_y
0.0	−0.0003	0.0006	0.0020
−2.0	.0014	−.0040	.0097
−4.0	.0031	−.0085	.0175
0*	0*	0*	0*
−2.0*	.0017*	−.0046*	.0079*
−4.0*	.0034*	−.0092*	.0158*

(c) $\alpha = -5°$

β, deg	C_l	C_n	C_y
0.0	−0.0001	0.0003	0.0019
−2.0	.0013	−.0035	.0095
−4.0	.0028	−.0076	.0174
0*	0*	0*	0*
−2.0*	.0015*	−.0041*	.0080*
−4.0*	.0030*	−.0081*	.0160*

Table VII. Measured Lateral and Directional Aerodynamic Characteristics in CF_4 for $M_\infty = 5.87$, $Re_\infty = 0.46 \times 10^6$/ft, $Re_{2,d} = 37\,000$, and $d = 2.50$ in.

[Numbers with asterisk are derived from curve through 0,0 in fig. 7]

(a) $\alpha = 0°$

β, deg	C_l	C_n	C_y
0	0.0000	0.0037	0.0017
0	.0008	.0036	.0021
2.50	−.0016	.0094	−.0084
2.50	−.0015	.0094	−.0086
5.0	−.0035	.0144	−.0179
5.0	−.0035	.0148	−.0187
−2.50	.0032	−.0028	.0136
−2.50	.0033	−.0029	.0136
−5.0	.0048	−.0084	.0234
−5.0	.0053	−.0085	.0237
0*	0*	0*	0*
−2.5*	.0024*	−.0064*	.0108*
2.5*	−.0024*	−.0064*	−.0108*
−5.0*	.0047*	−.00128*	.0215*
5.0*	−.0047*	.00128*	−.0215*

(b) $\alpha = 5°$

β, deg	C_l	C_n	C_y
0.0	0.0007	0.0035	0.0026
2.50	−.0012	.0084	−.0061
5.0	−.0030	.0133	−.0152
−2.50	.0027	−.0018	.0121
−5.0	.0046	−.0066	.0212
0*	0*	0*	0*
−2.5*	.0020*	−.0050*	.0093*
2.5	−.0020*	−.0050*	−.0093*
−5.0*	.0039*	−.0099*	.0185*
5.0*	−.0039*	.0099*	−.0185*

Table VII. Continued

(c) $\alpha = -5°$

β, deg	C_l	C_n	C_y
0.0	0.0008	0.0035	0.0018
2.50	−.0014	.0091	−.0094
5.0	−.0037	.0159	−.0216
−2.50	.0033	−.0028	.0138
−5.0	.0053	−.0083	.0245
0*	0*	0*	0*
−2.5*	.0023*	−.0060*	.0115*
2.5*	−.0023*	−.0060*	−.0115*
−5.0*	.0045*	−.00120*	.0230*
5.0*	−.0045*	.00120*	−.0230*

(d) $\alpha = 10°$

β, deg	C_l	C_n	C_y
0.0	0.0007	0.0034	0.0027
2.50	−.0011	.0084	−.0060
5.0	−.0030	.0137	−.0152
−2.50	.0026	−.0018	.0123
−5.0	.0045	−.0070	.0214
0*	0*	0*	0*
−2.5*	.0019*	−.0050*	.0093*
2.5*	−.0019*	.0050*	−.0093*
−5.0*	.0037*	−.00100*	.0185*
5.0*	−.0037*	.00100*	−.0185*

Table VII. Concluded

(e) $\alpha = -10^\circ$

β, deg	C_l	C_n	C_y
0.0	0.0011	0.0035	0.0010
2.50	−.0011	.0086	−.0101
5.0	−.0029	.0138	−.0213
−2.50	.0031	−.0041	.0131
−5.0	.0049	−.0078	.0248
0*	0*	0*	0*
−2.5*	.0020*	−.0053*	.0118*
2.5*	−.0020*	.0053*	−.0118*
−5.0*	.0040*	−.00106*	.0235*
5.0*	−.0040*	.00106*	−.0235*

Table VIII. Lateral and Directional Stability Characteristics

(a) $M_\infty = 9.90$; $Re_\infty = 1.09 \times 10^6$/ft; $Re_{2,d} = 18\,042$; $d = 2.50$ in.; air as test gas

α, deg	C_{y_β}, deg^{-1}	C_{n_β}, deg^{-1}	C_{l_β}, deg^{-1}
−9.80	−0.004663	0.002299	−0.000834
−4.77	−.003730	.001942	−.000682
−2.31	−.004249	.002040	−.000699
.21	−.003700	.001887	−.000725
2.73	−.003785	.002010	−.000760
5.26	−.004203	.002258	−.000821
10.35	−.004163	.002585	−.000908

(b) $M_\infty = 5.84$; $Re_\infty = 0.63 \times 10^6$/ft; $Re_{2,d} = 29\,400$; $d = 3.67$ in.; air as test gas

α, deg	C_{y_β}, deg^{-1}	C_{n_β}, deg^{-1}	C_{l_β}, deg^{-1}
−5.0	−0.0040	0.0020	−0.00075
0	−.0040	.0021	−.00075
5.0	−.0040	.0023	−.00084

(c) $M_\infty = 5.94$; $Re_\infty = 2.21 \times 10^6$/ft; $Re_{2,d} = 107\,000$; $d = 3.67$ in.; air as test gas

α, deg	C_{y_β}, deg^{-1}	C_{n_β}, deg^{-1}	C_{l_β}, deg^{-1}
−5.0	−0.0040	0.0020	−0.00075
0	−.0040	.0021	−.00075
5.0	−.0040	.0023	−.00084

(d) $M_\infty = 5.87$; $Re_\infty = 0.46 \times 10^6$/ft; $Re_{2,d} = 37\,000$; $d = 2.50$ in.; CF_4 as test gas

α, deg	C_{y_β}, deg^{-1}	C_{n_β}, deg^{-1}	C_{l_β}, deg^{-1}
−10.0	−0.0047	0.00212	−0.00080
−5.0	−.0046	.00240	−.00090
0	−.0043	.00256	−.00094
5.0	−.0037	.00198	−.00078
10.0	−.0037	.00200	−.00074

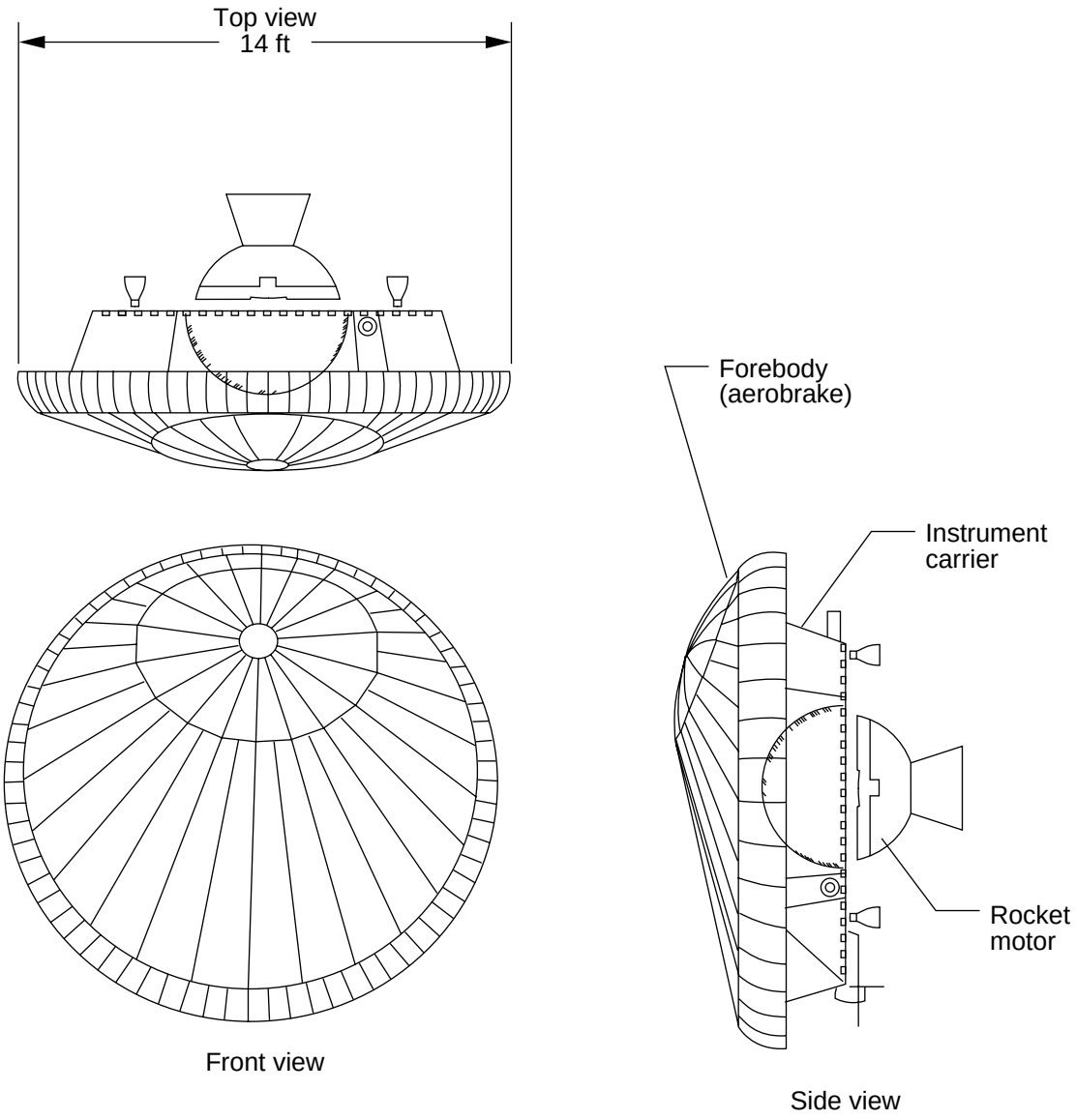

Figure 1. AFE flight vehicle configuration.

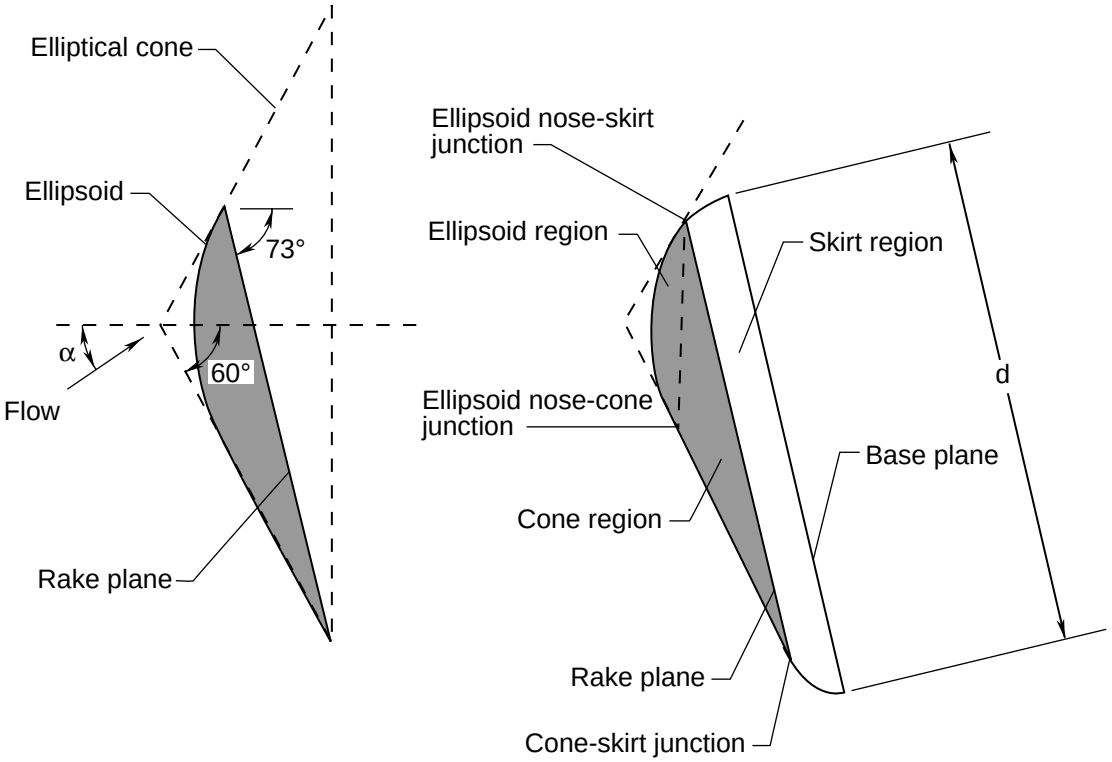

Figure 2. AFE vehicle forebody development from elliptical cone.

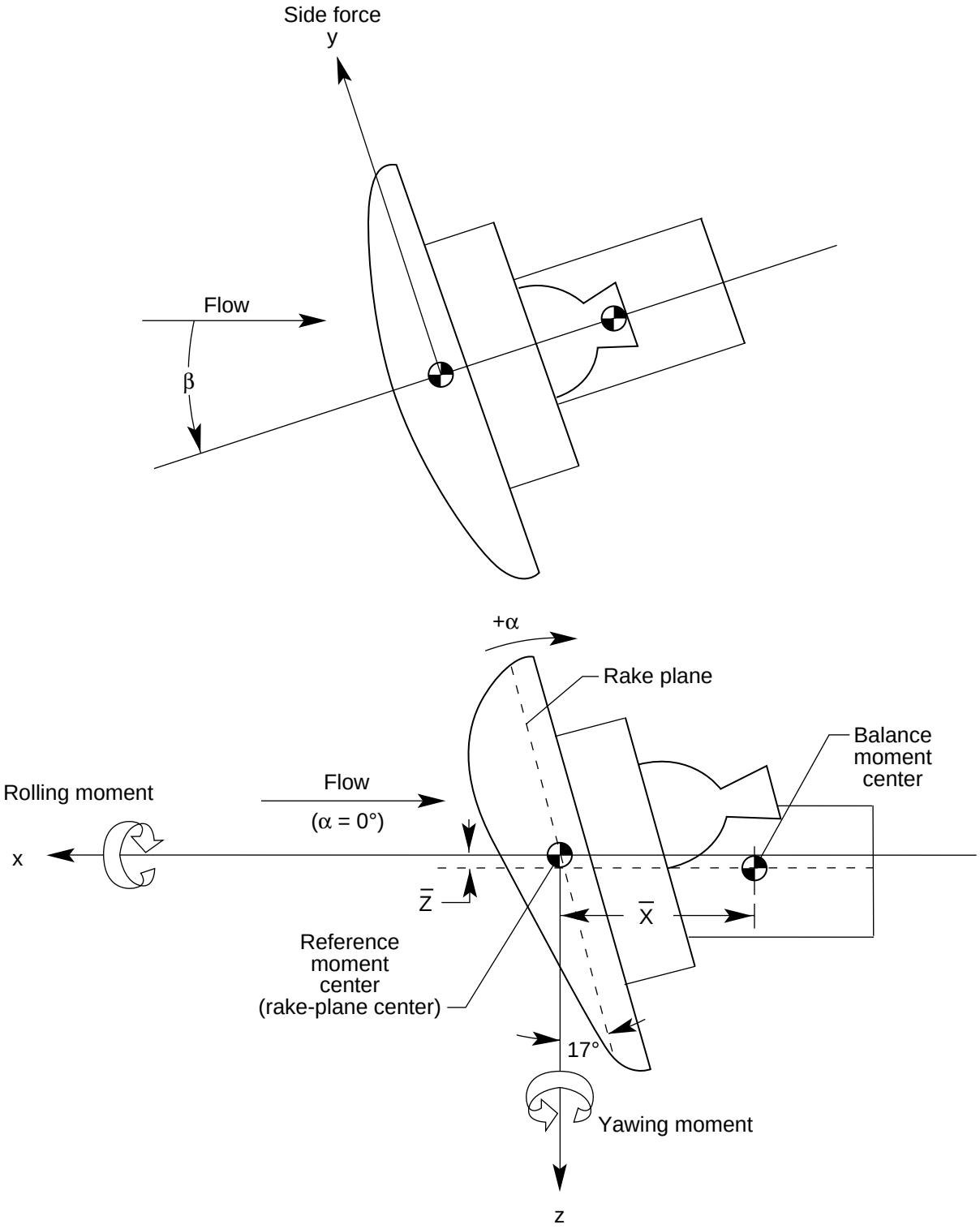

Figure 4. System of axes with positive direction of forces, moments, velocities, and angles indicated.

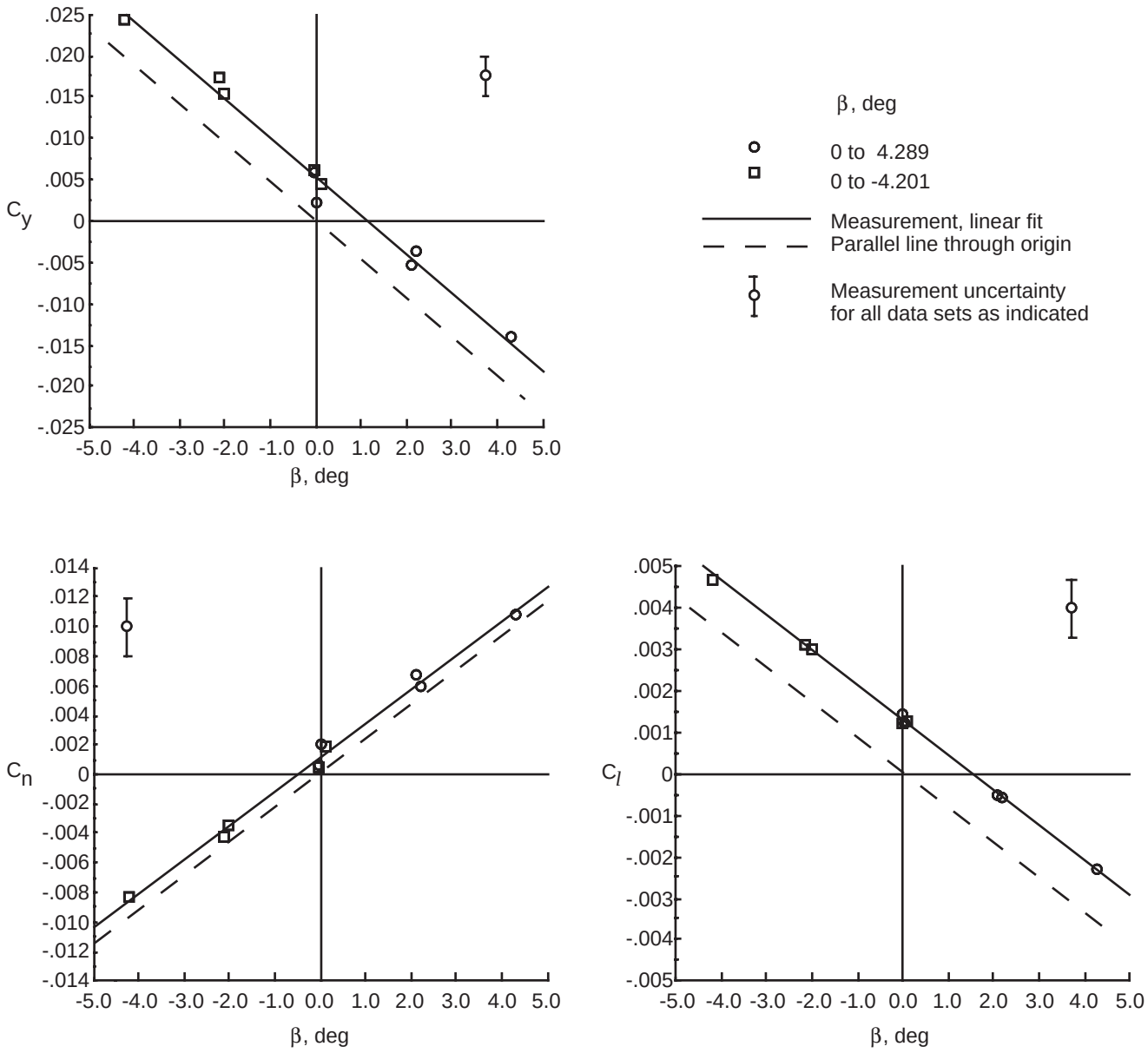

(a) $\alpha = -10.0°$.

Figure 5. Variation of lateral and directional aerodynamic characteristics with angle of sideslip in air at $M_\infty = 9.90$ and $Re_\infty = 1.09 \times 10^6$/ft.

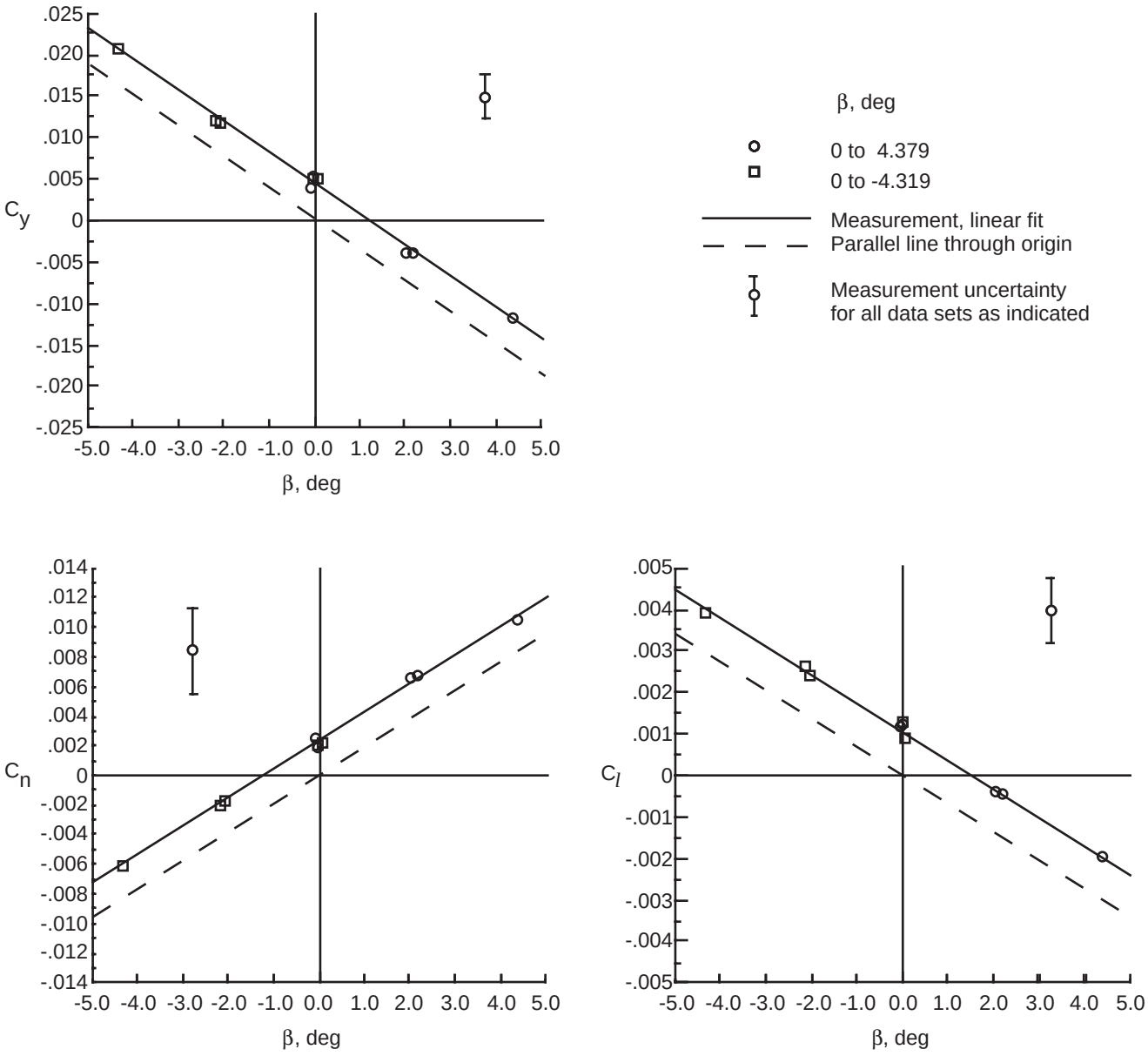

(b) $\alpha = -5.0°$.

Figure 5. Continued.

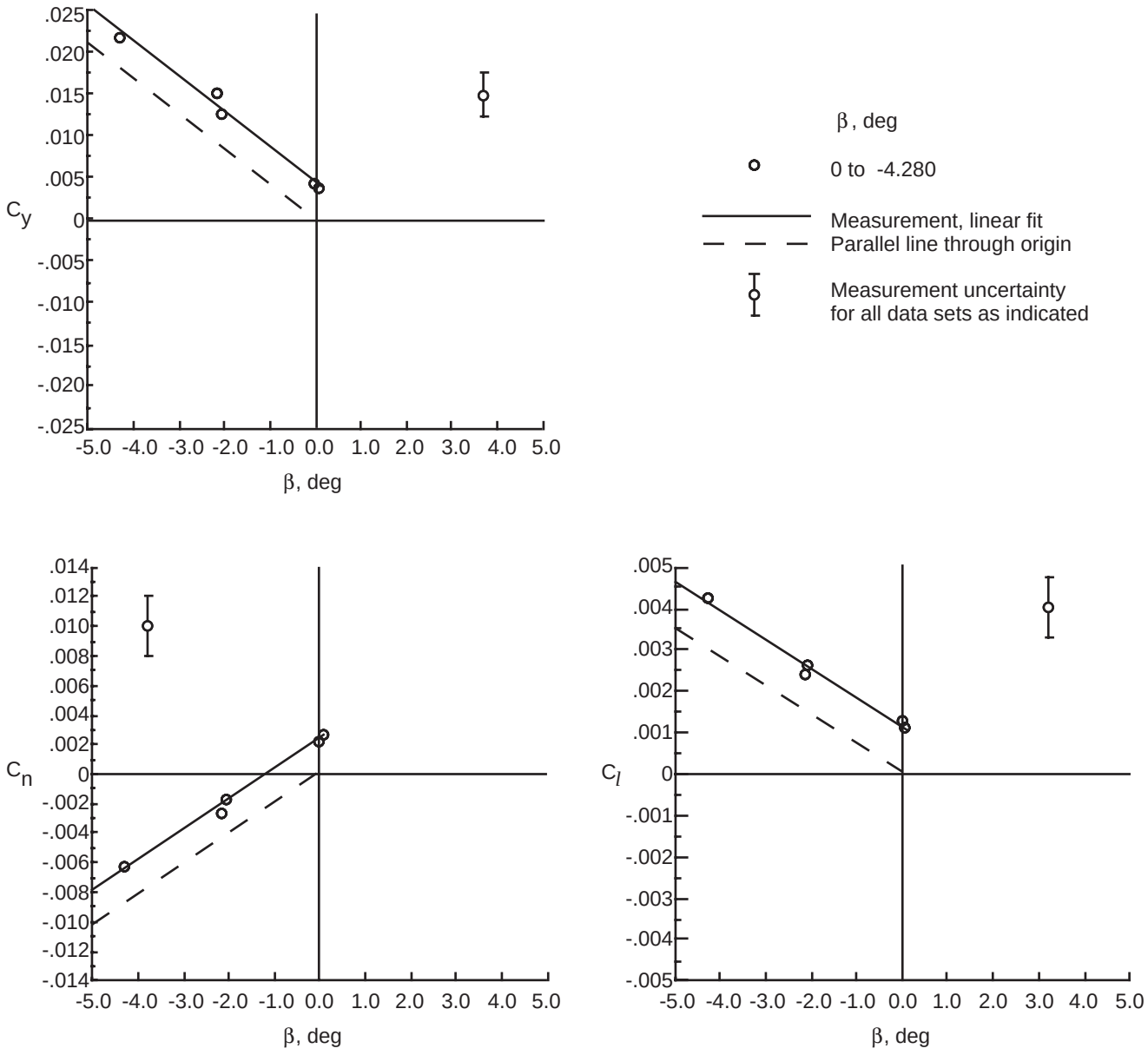

(c) $\alpha = -2.5°$.

Figure 5. Continued.

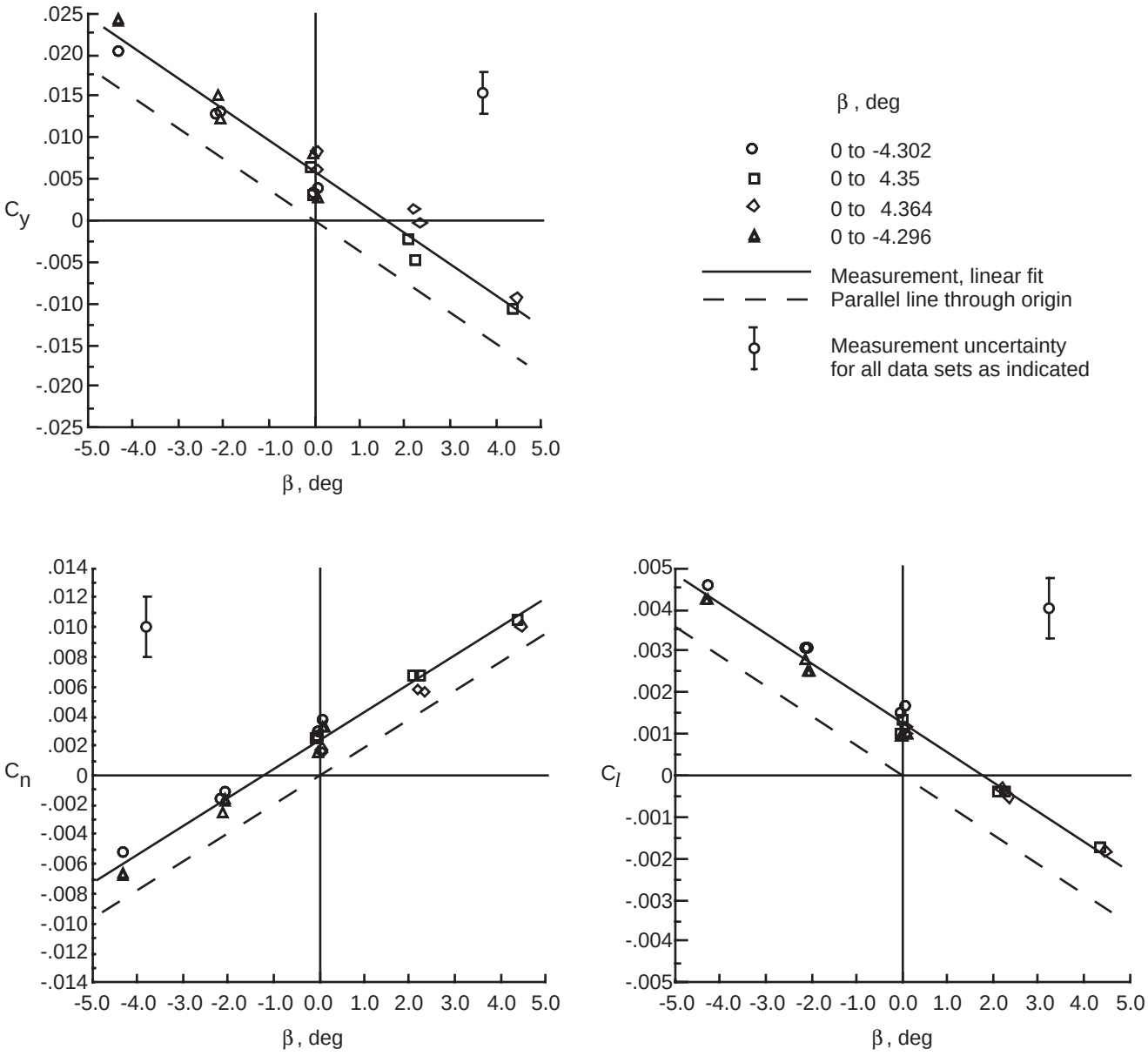

(d) $\alpha = 0°$.

Figure 5. Continued.

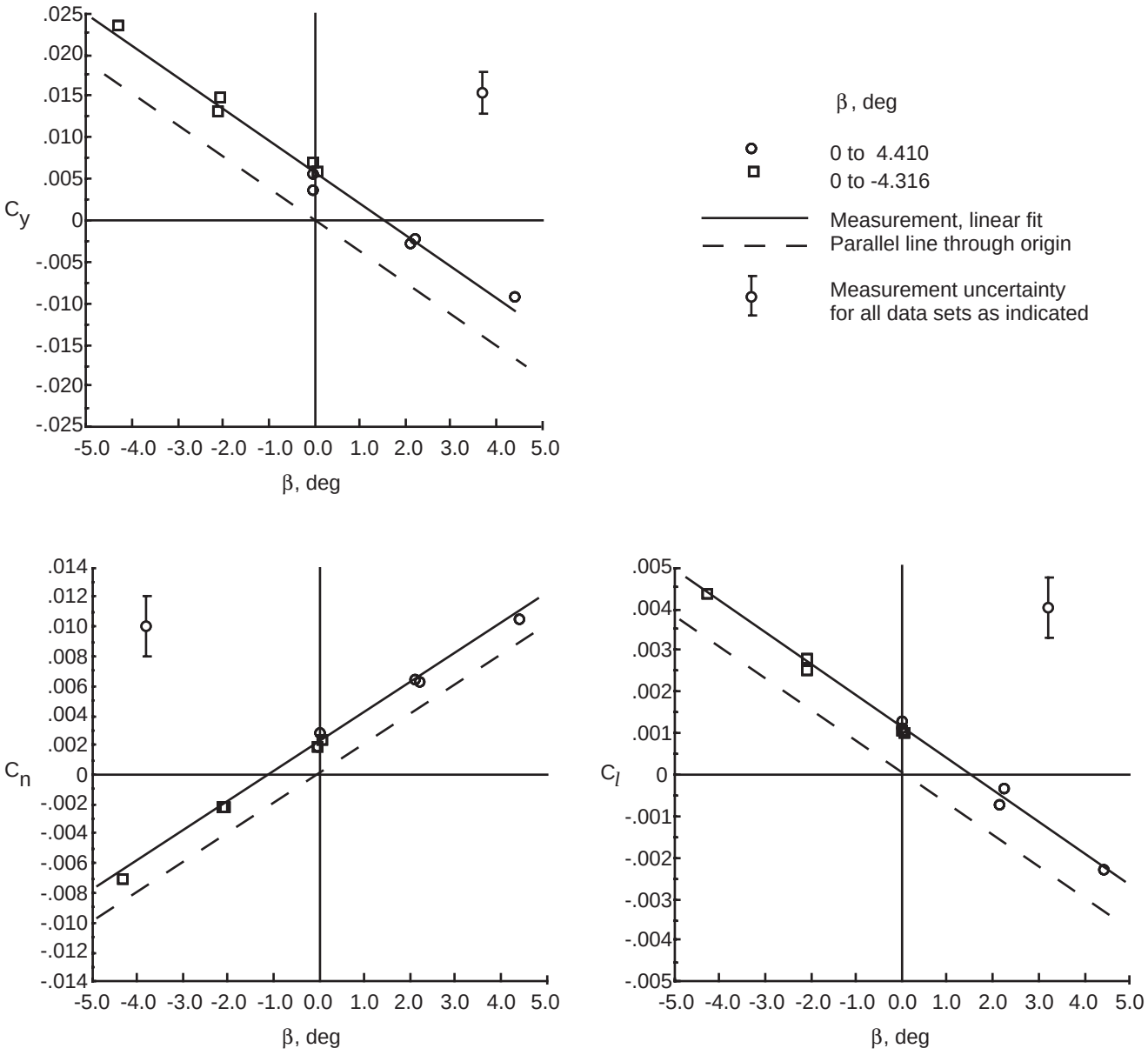

(e) $\alpha = 2.5°$.

Figure 5. Continued.

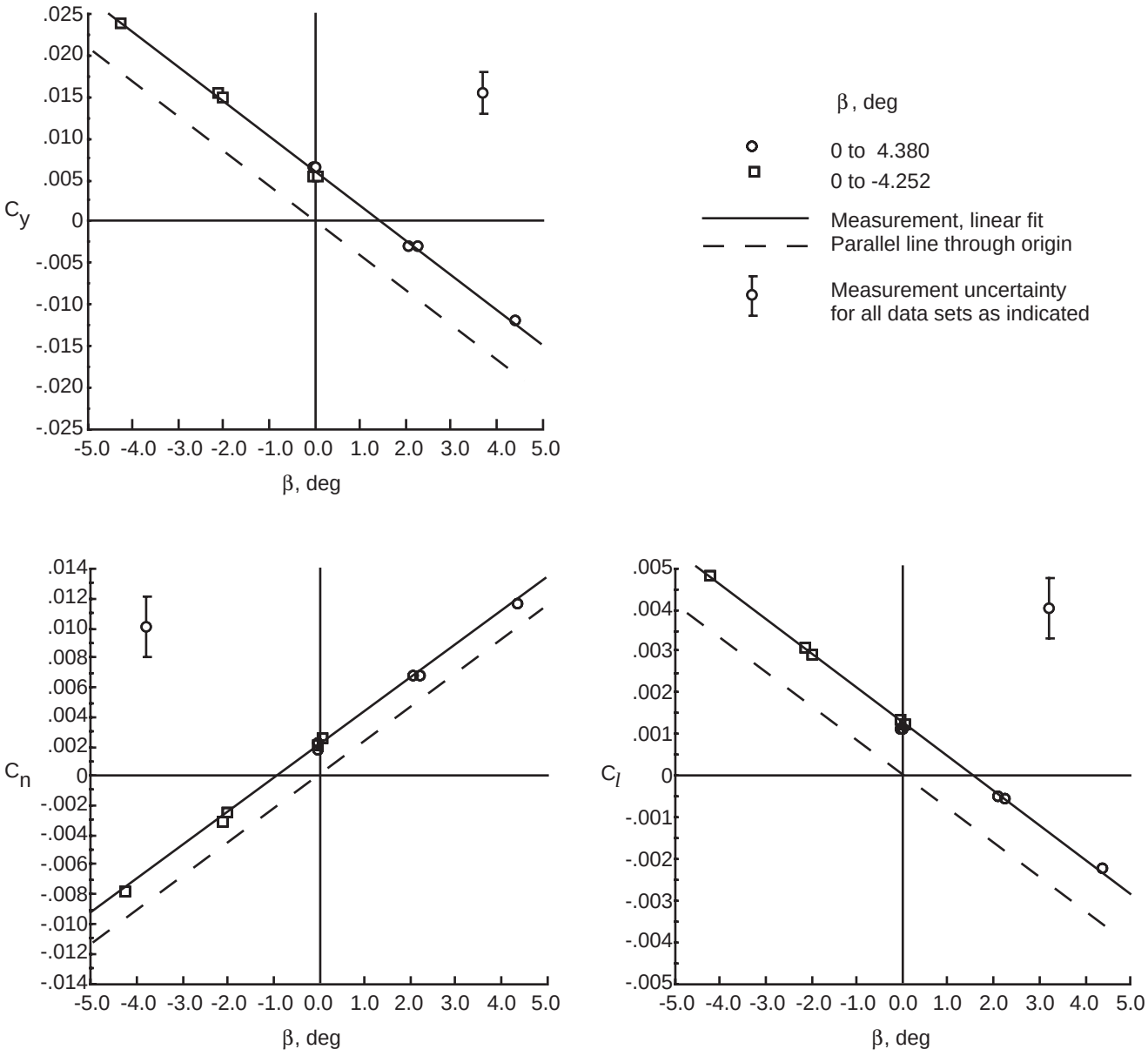

(f) $\alpha = 5.0°$.

Figure 5. Continued.

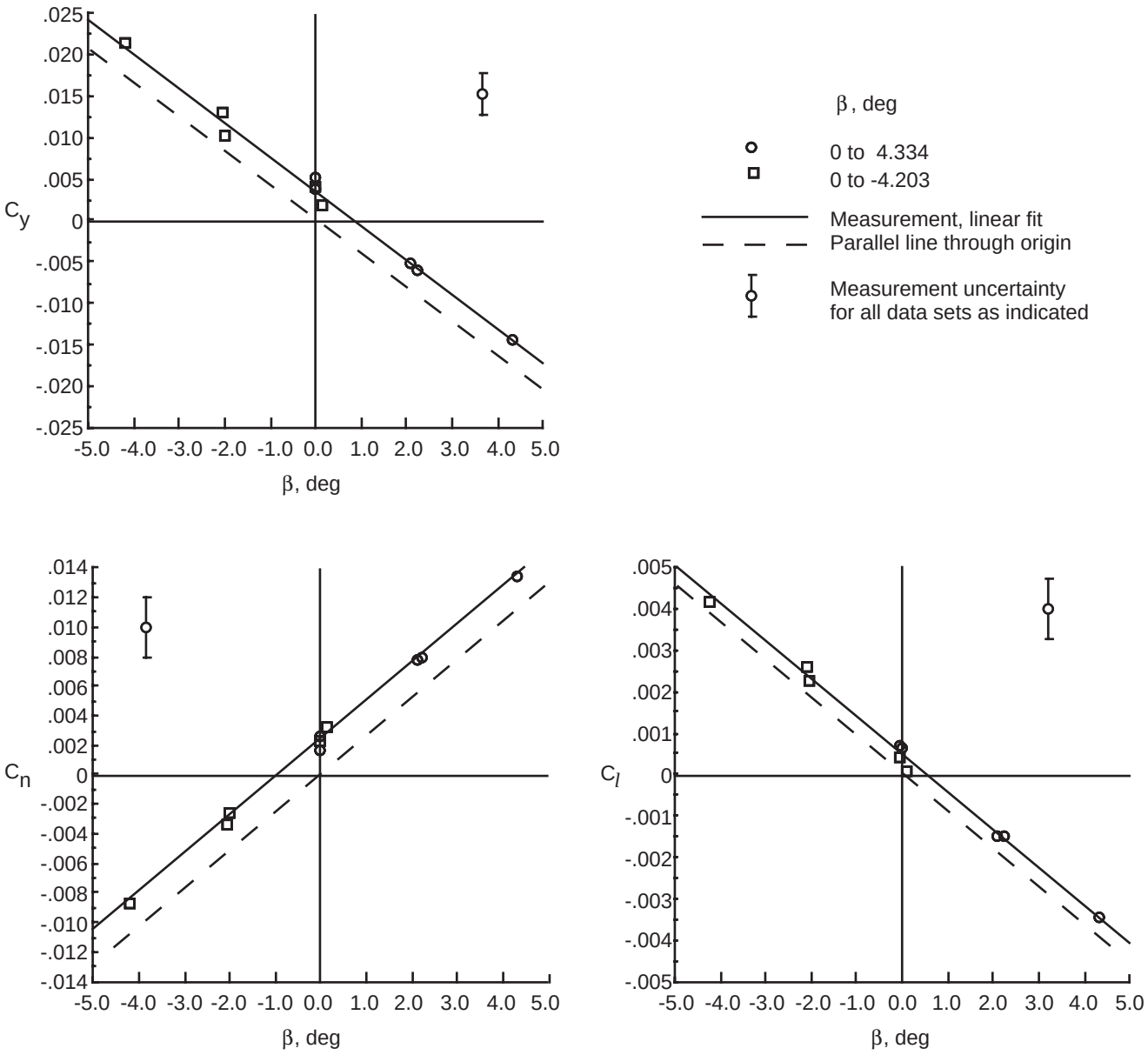

(g) $\alpha = 10.0°$.

Figure 5. Concluded.

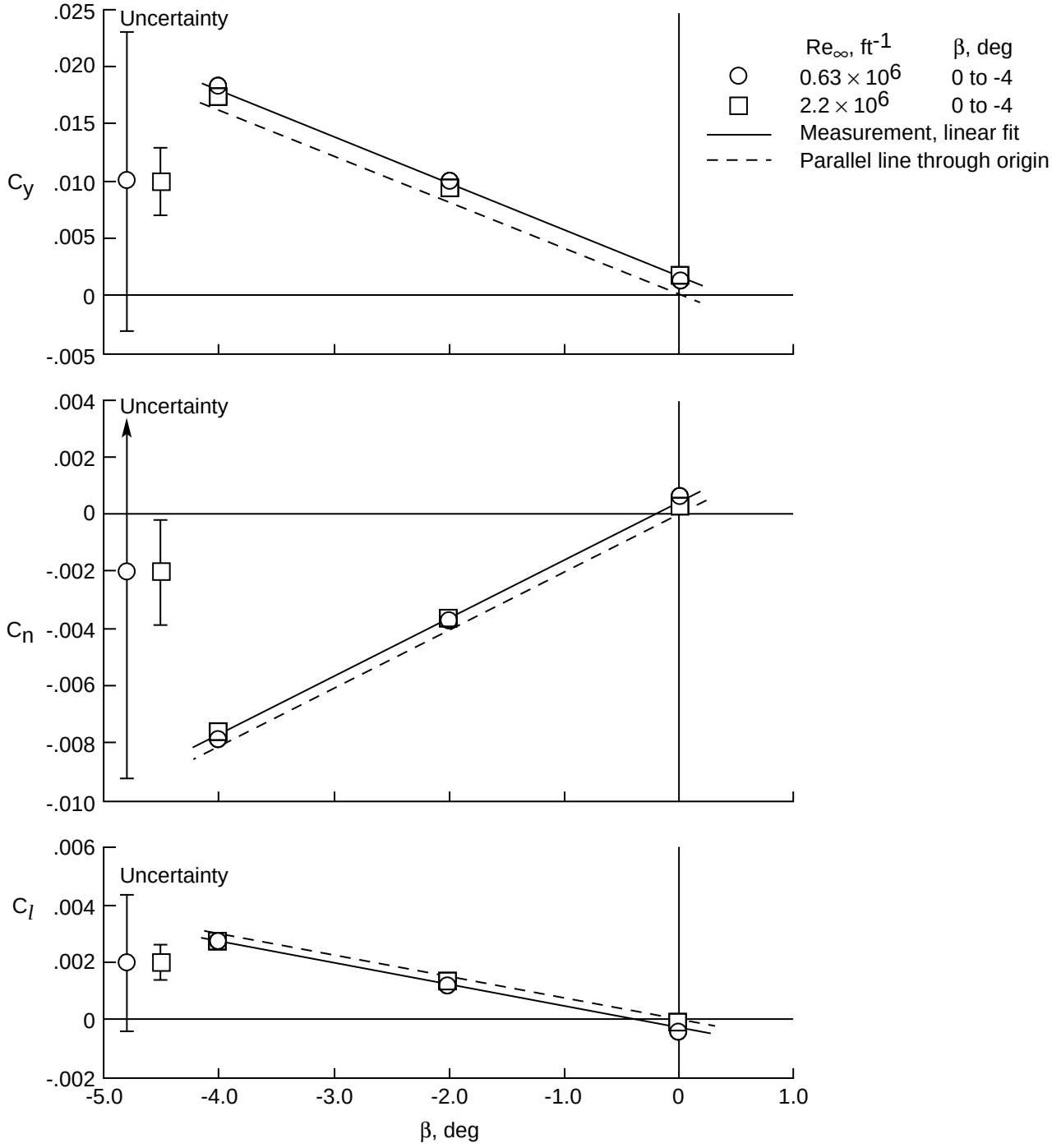

(a) $\alpha = -5°$.

Figure 6. Variation of lateral and directional aerodynamic characteristics with angle of sideslip in air at $M_\infty = 6$ for two values of Re_∞.

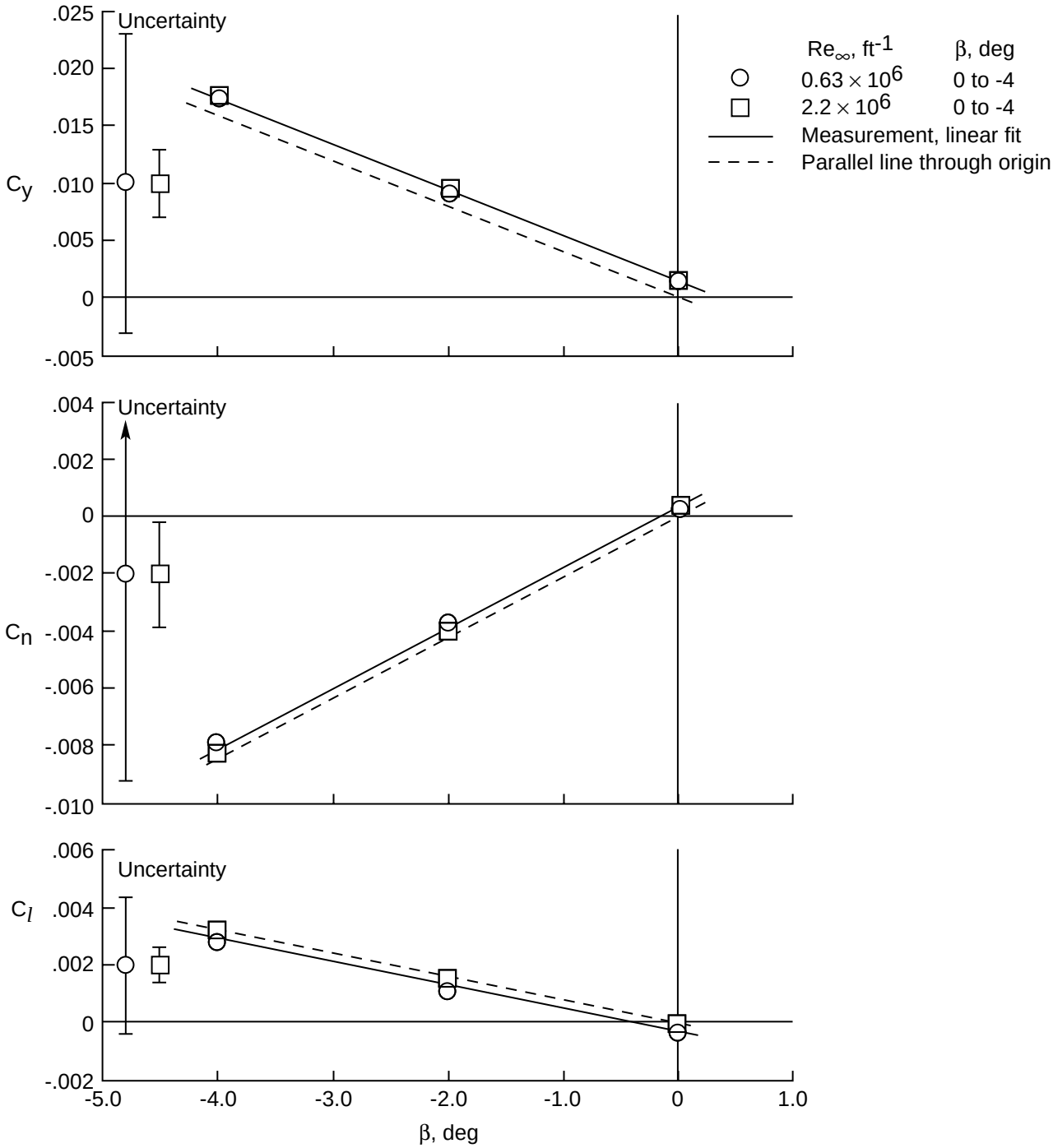

(b) $\alpha = 0°$.

Figure 6. Continued.

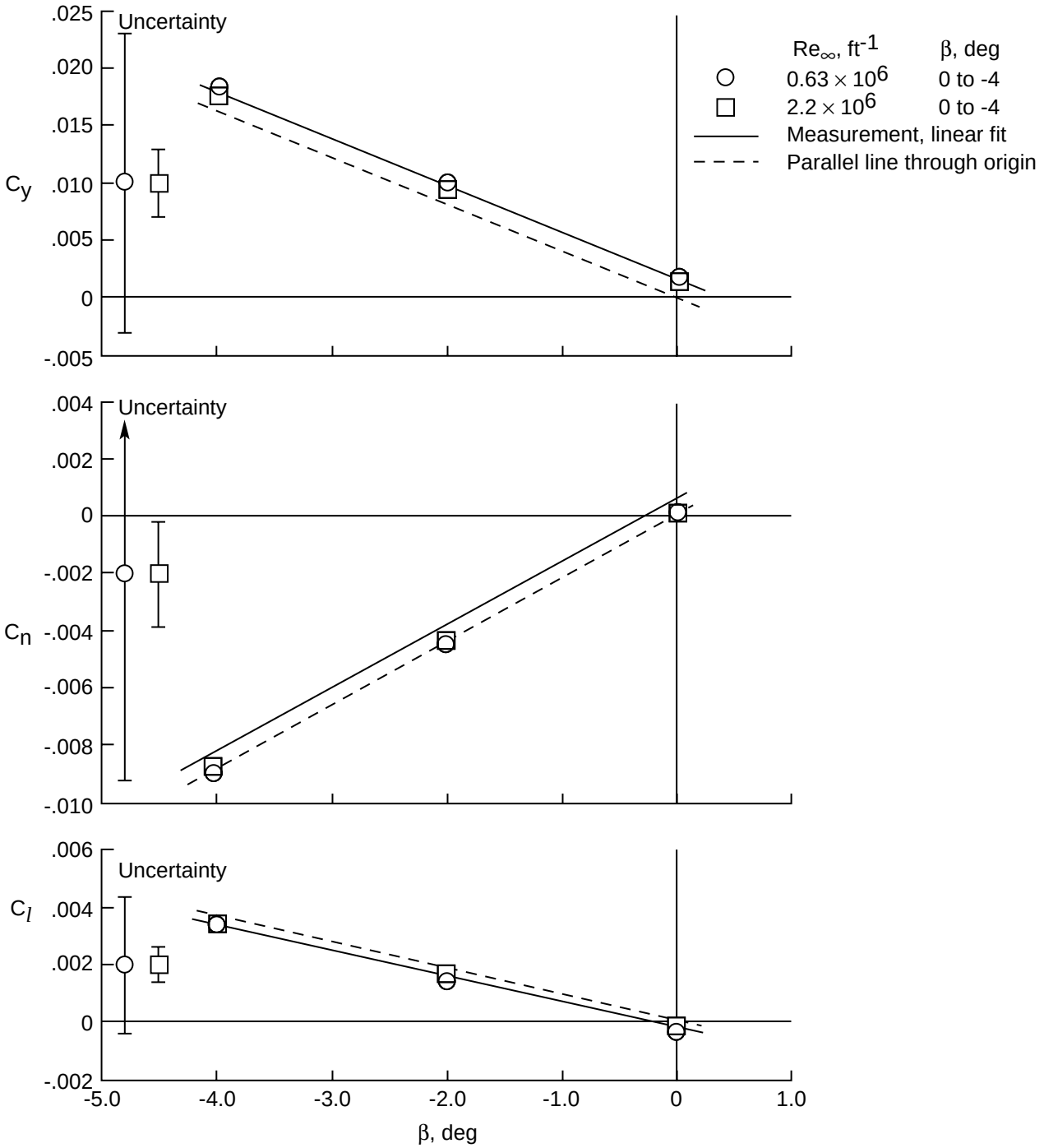

(c) $\alpha = 5°$.

Figure 6. Concluded.

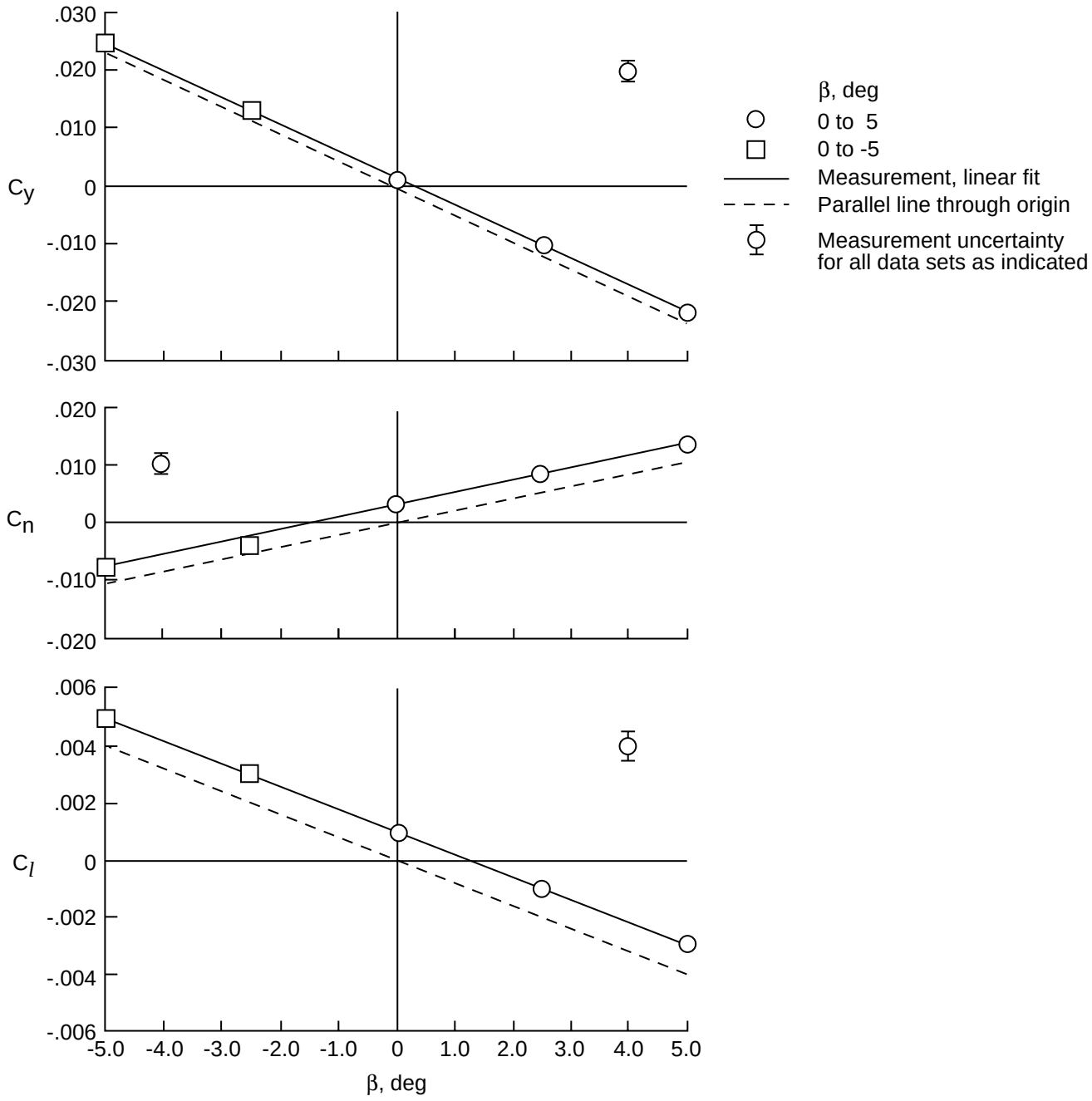

(a) $\alpha = -10°$.

Figure 7. Variation of lateral and directional aerodynamic characteristics with angle of sideslip in CF_4 at $M_\infty = 6$ and $Re_\infty = 0.46 \times 10^6$/ft.

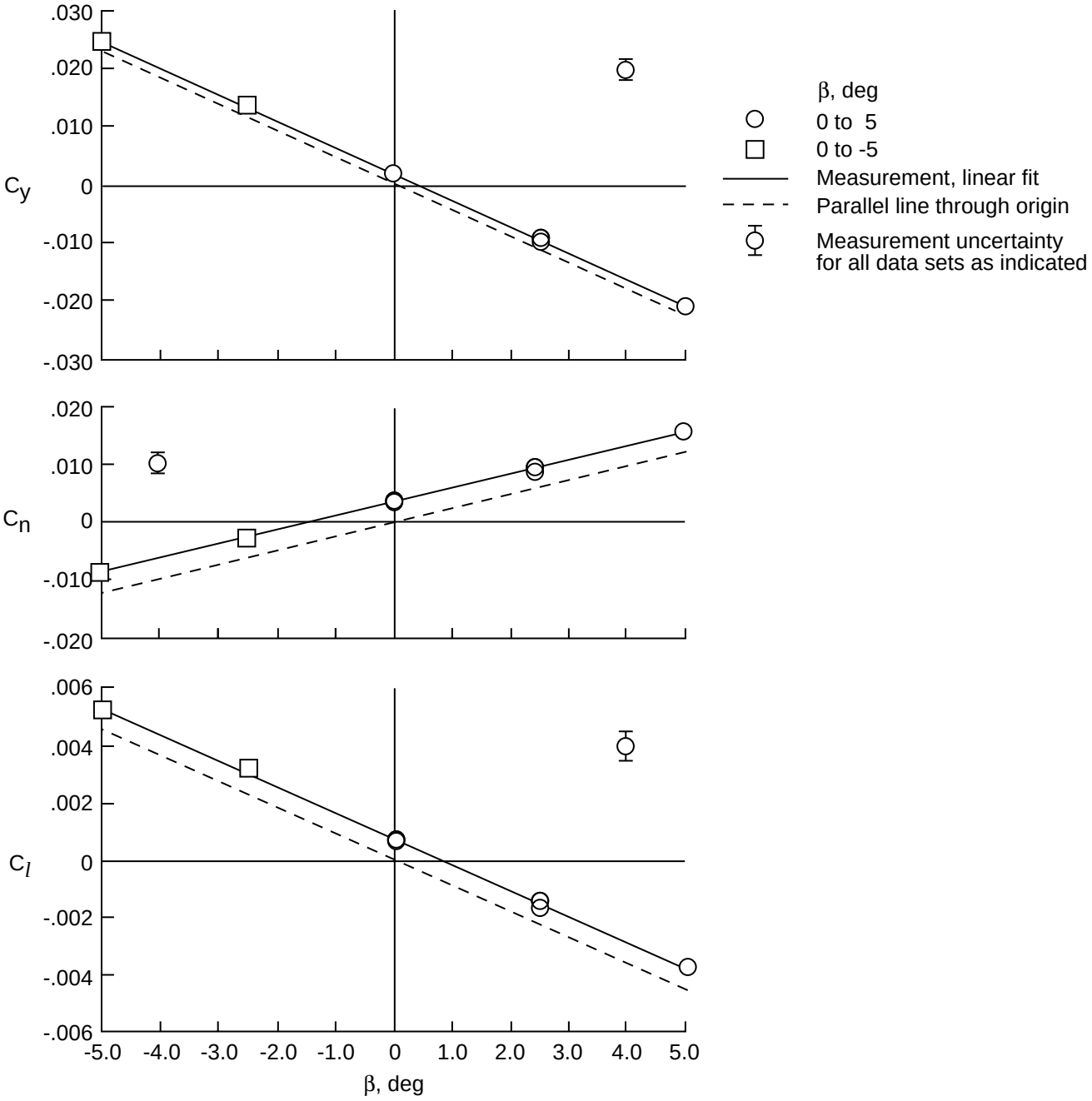

(b) $\alpha = -5°$.

Figure 7. Continued.

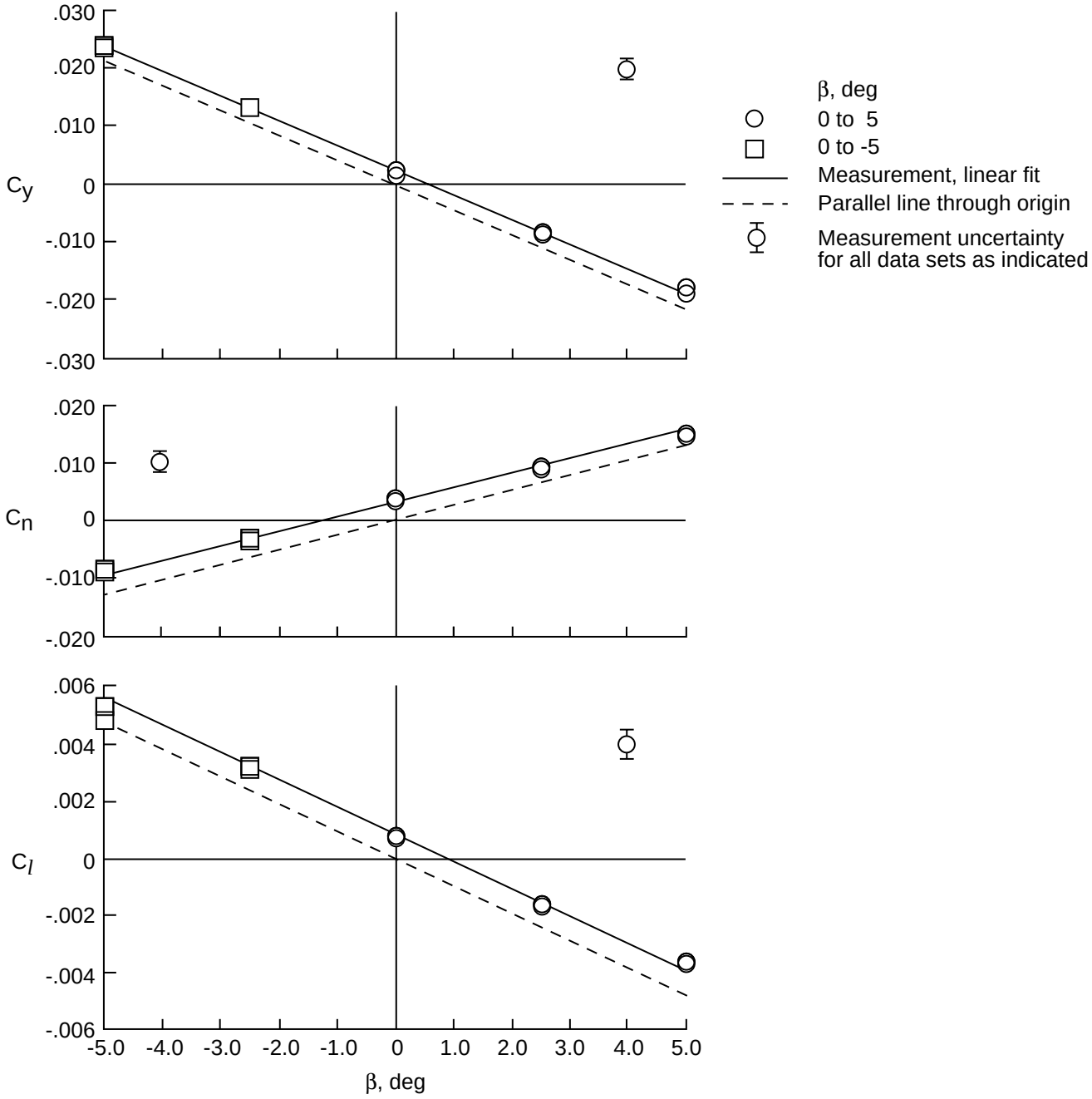

(c) $\alpha = 0°$.

Figure 7. Continued.

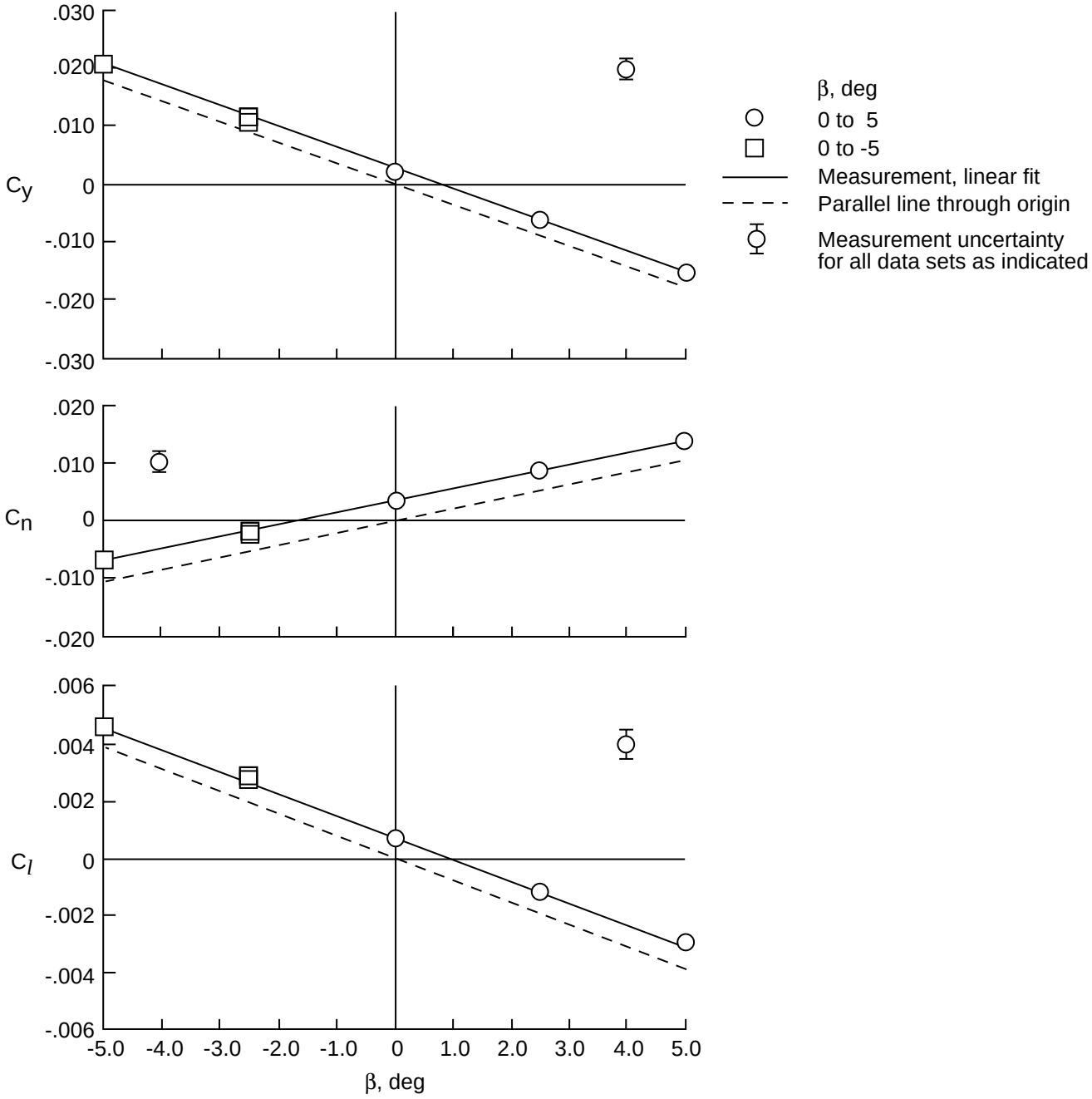

(d) $\alpha = 5°$.

Figure 7. Continued.

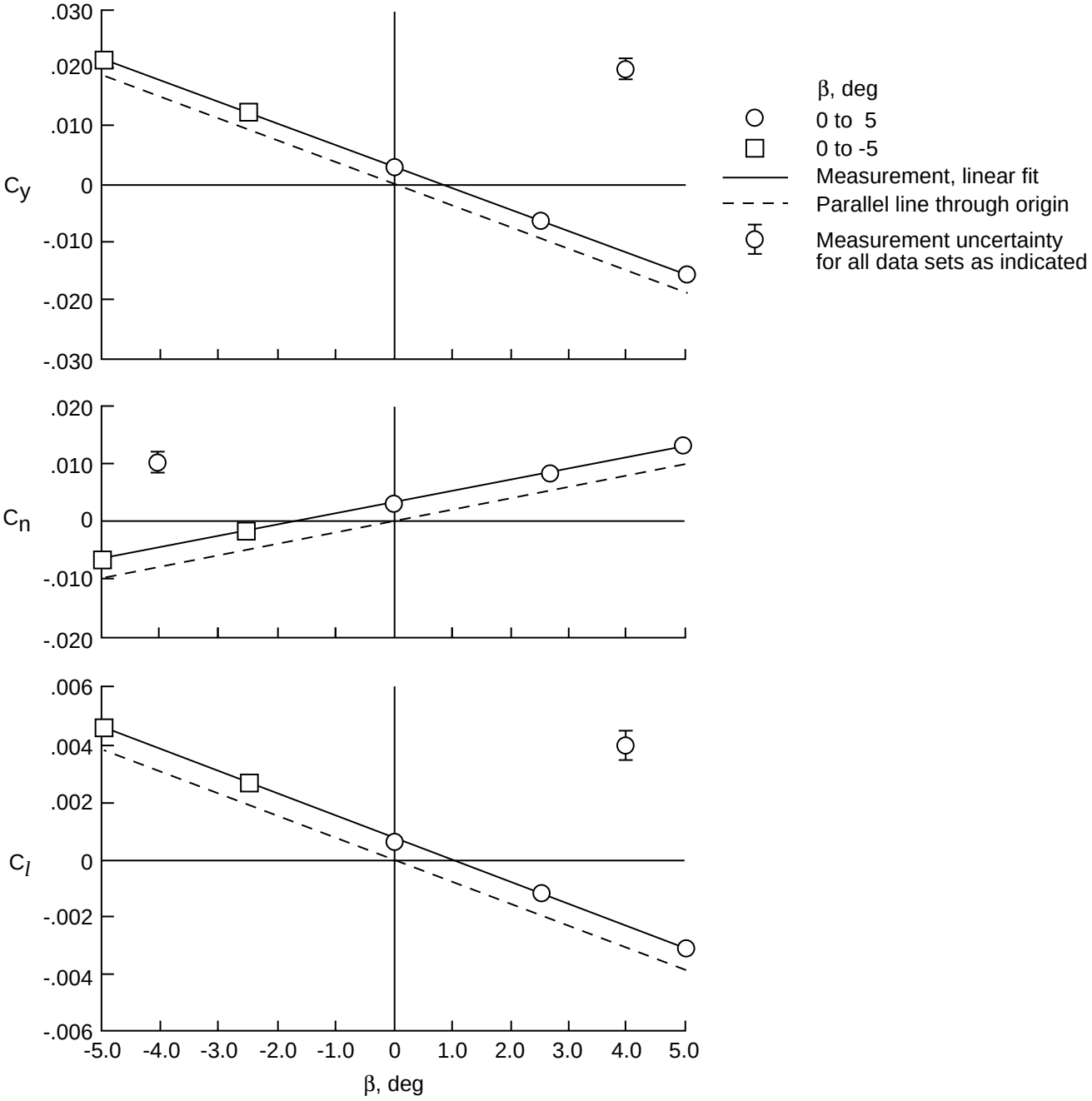

(e) $\alpha = 10°$.

Figure 7. Concluded.

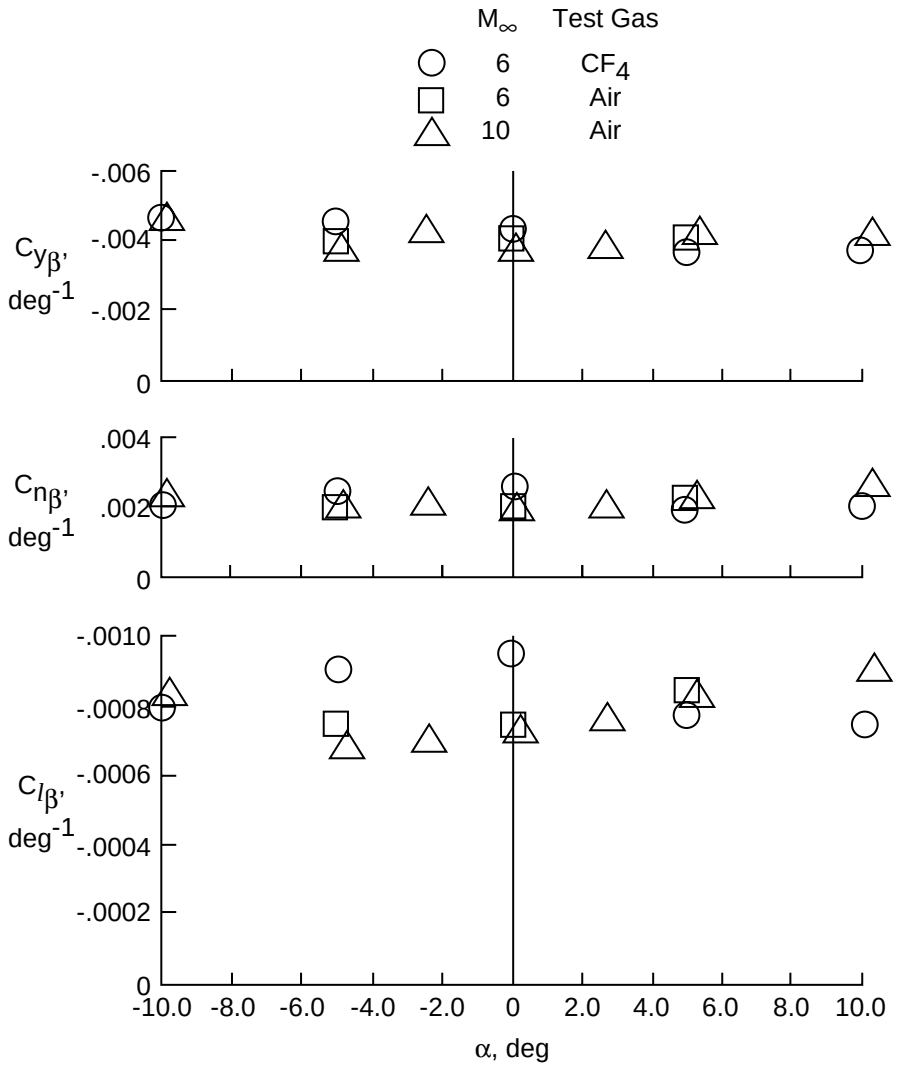

Figure 8. Lateral and directional stability characteristics in air and CF_4. Note sign change in top and bottom figures.

L-87-04291

(a) The 3.67-in-diameter model, aftbody, and balance holder.

Figure 3. The AFE models used in lateral and directional aerodynamics tests.

L-90-11872

(b) The 2.50-in-diameter model and balance shroud.

Figure 3. Continued.

L-90-14502

(c) The 2.50-in-diameter model mounted in Langley 20-Inch Mach 6 CF_4 Tunnel.

Figure 3. Concluded.

REPORT DOCUMENTATION PAGE

Form Approved
OMB No. 0704-0188

1. AGENCY USE ONLY *(Leave blank)*	2. REPORT DATE	3. REPORT TYPE AND DATES COVERED
	May 1993	Technical Memorandum

4. TITLE AND SUBTITLE
Hypersonic Lateral and Directional Stability Characteristics of Aeroassist Flight Experiment Configuration in Air and CF_4

5. FUNDING NUMBERS
WU 506-40-41-01

6. AUTHOR(S)
John R. Micol and William L. Wells

7. PERFORMING ORGANIZATION NAME(S) AND ADDRESS(ES)
NASA Langley Research Center
Hampton, VA 23681-0001

8. PERFORMING ORGANIZATION REPORT NUMBER
L-17154

9. SPONSORING/MONITORING AGENCY NAME(S) AND ADDRESS(ES)
National Aeronautics and Space Administration
Washington, DC 20546-0001

10. SPONSORING/MONITORING AGENCY REPORT NUMBER
NASA TM-4435

11. SUPPLEMENTARY NOTES

12a. DISTRIBUTION/AVAILABILITY STATEMENT
Unclassified–Unlimited

Subject Category 02

12b. DISTRIBUTION CODE

13. ABSTRACT *(Maximum 200 words)*

Hypersonic lateral and directional stability characteristics measured on a 60° half-angle elliptical cone, which was raked at an angle of 73° from the cone centerline and with an ellipsoid nose (ellipticity equal to 2.0 in the symmetry plane), are presented for angles of attack from −10° to 10°. The high normal-shock density ratio of a real gas was simulated by tests at a Mach number of 6 in air and CF_4 (density ratio equal to 5.25 and 12.0, respectively). Tests were conducted in air at Mach 6 and 10 and in CF_4 at Mach 6 to examine the effects of Mach number, Reynolds number, and normal-shock density ratio. Changes in Mach number from 6 to 10 in air or in Reynolds number by a factor of 4 at Mach 6 had a negligible effect on lateral and directional stability characteristics. Variations in normal-shock density ratio had a measurable effect on lateral and directional aerodynamic coefficients, but no significant effect on lateral and directional stability characteristics. Tests in air and CF_4 indicated that the configuration was laterally and directionally stable through the test range of angle of attack.

14. SUBJECT TERMS	15. NUMBER OF PAGES
AFE; Aerodynamics; Real-gas simulation; Hypersonic; Blunt body	40
	16. PRICE CODE: A03

17. SECURITY CLASSIFICATION OF REPORT	18. SECURITY CLASSIFICATION OF THIS PAGE	19. SECURITY CLASSIFICATION OF ABSTRACT	20. LIMITATION OF ABSTRACT
Unclassified	Unclassified		